Final Technical Report

Grant No. AFOSR F49620-01-1-0474

Surface Modification Engineered Assembly of Novel Quantum Dot Architectures for Advanced Applications

Period: July 1, 2001- June 30, 2007

Program Managers: Gernot Pomrenke (AFSOR) & Dan Radack (DARPA)

PI:
Anupam Madhukar
University of Southern California
Los Angeles, CA 90089-0241
Tel. (213) 740-4325
email: madhukar@usc.edu

Co-PIs:
R. Kalia, USC
A. Nakano, USC
D. H. Rich, USC
P. Vashishta, USC
A. Paul Alivisatos, UC Berkeley
S. Chou, Princeton

Abstract: This DURINT program proposed and undertook several ground-breaking efforts aimed at exploring novel and innovative composite nanostructures created from the integration of the two classes of nanostuctures - the epitaxial nanostructures (e.g quantum wells) and the nanocrystal quantum structures (e.g. quantum dots). This Final Technical Report summarizes the objectives pursued and major accomplishments. The highlights include the following firsts: (1) demonstration of nonradiative resonant excitation transfer from adsorbed NCQDs to adjacent buried nanostructure, thus opening a new paradigm for potentially high efficiency solar cells; (2) demonstration of epitaxial overgrowth on adsorbed nanocrystals; (3) demonstration of CdTe tetrapod single electron transistors; (4) molecular dynamics simulations of organic PEG-conjugated SAMs on Au and GaAs; (5) demonstration of metallic nanoparticles based plasmon ruler; (6) atomic-scale characterization of adsorbed peptide-conjugated SAMs and their role in specific adhesion of cells; (7) simultaneous nanoscale spatially-resolved measurement of morphology and luminescence from living cells; (8) synthesis and photoresponse measurement of semiconductor (CdSe)-metal (Au) epitaxial composite nanocrystal Schottky junction.

REPORT DOCUMENTATION PAGE

Form Approved
OMB No. 0704-0188

PLEASE DO NOT RETURN YOUR FORM TO THE ABOVE ORGANIZATION.

1. REPORT DATE *(DD-MM-YYYY)*	2. REPORT TYPE	3. DATES COVERED *(From - To)*
09/02/08	Final Technical Report	July 1, 2001 - June 30, 2007

4. TITLE AND SUBTITLE
Surface Modification Engineered Assembly of Novel Quantum Dot Architectures for Advanced Applications

5a. CONTRACT NUMBER
F49620-01-1-0474

5b. GRANT NUMBER
AFOSR F49620-01-1-0474

5c. PROGRAM ELEMENT NUMBER

6. AUTHOR(S)
Madhukar, Anupam; Lu, Siyuan; Alivisatos, Paul; Vashishta, Priya; Kalia, Rajiv; Nakano, Aiichiro

5d. PROJECT NUMBER

5e. TASK NUMBER

5f. WORK UNIT NUMBER

7. PERFORMING ORGANIZATION NAME(S) AND ADDRESS(ES)
University of Southern California
Department of Chemical Engineering and Materials Science
3651 Watt Way, VHE 506
Los Angeles, CA 90089-0241

8. PERFORMING ORGANIZATION REPORT NUMBER

9. SPONSORING/MONITORING AGENCY NAME(S) AND ADDRESS(ES)
AFOSR/NE
110 Duncan Ave. Suite B115
Bolling AFB, DC 20332-8050

10. SPONSOR/MONITOR'S ACRONYM(S)

11. SPONSOR/MONITOR'S REPORT NUMBER(S)
AFRL-SR-AR-TR-08-0531

12. DISTRIBUTION/AVAILABILITY STATEMENT
Approved for public release; distribution unlimited.

13. SUPPLEMENTARY NOTES
The view, opinion, and/or findings in this report are those of the author(s) and should not be constructed as an official Department of the Air Force position, policy, or decision, unless so designated by other documentation.

14. ABSTRACT
This DURINT program proposed and undertook several ground-breaking efforts aimed at exploring novel and innovative composite nanostructures created from the integration of the two classes of nanostuctures - the epitaxial nanostructures (e.g quantum wells) and the nanocrystal quantum structures (e.g. quantum dots). This Final Technical Report summarizes the objectives pursued and major accomplishments. The highlights include the following firsts: (1) demonstration of nonradiative resonant excitation transfer from adsorbed NCQDs to adjacent buried nanostructure, thus opening a new paradigm for potentially high efficiency solar cells; (2) demonstration of epitaxial overgrowth on adsorbed nanocrystals; (3) demonstration of CdTe tetrapod single electron transistors; (4) molecular dynamics simulations of organic PEG-conjugated SAMs on Au and GaAs; (5) demonstration of metallic nanoparticles based plasmon ruler; (6) atomic-scale characterization of adsorbed peptide-conjugated SAMs and their role in specific adhesion of cells; (7) simultaneous nanoscale spatially-resolved measurement of morphology and luminescence from living cells; (8) synthesis and photoresponse measurement of semiconductor (CdSe)-metal (Au) epitaxial composite nanocrystal Schottky junction.

15. SUBJECT TERMS
Nanocrystal quantum dots, tetrapod transistors, self-assembled quantum dots, quantum wells, self-assembled monolayers, integrated hybrid nanocrystal-epitaxial quantum well / wire nanostructures, semiconductor-metal epitaxial nanocomposites, optical spectroscopy, electron microscopy, molecular dynamics, energy transfer, surface modification / functionalization, cell adhesion, biosensor, solar energy conversion

16. SECURITY CLASSIFICATION OF:			17. LIMITATION OF ABSTRACT	18. NUMBER OF PAGES	19a. NAME OF RESPONSIBLE PERSON
a. REPORT	b. ABSTRACT	c. THIS PAGE			Anupam Madhukar
Unclassified	Unclassified	Unclassified	UU	56	19b. TELEPHONE NUMBER *(Include area code)* 213-740-4323

Reset

INSTRUCTIONS FOR COMPLETING SF 298

1. REPORT DATE. Full publication date, including day, month, if available. Must cite at least the year and be Year 2000 compliant, e.g. 30-06-1998; xx-06-1998; xx-xx-1998.

2. REPORT TYPE. State the type of report, such as final, technical, interim, memorandum, master's thesis, progress, quarterly, research, special, group study, etc.

3. DATES COVERED. Indicate the time during which the work was performed and the report was written, e.g., Jun 1997 - Jun 1998; 1-10 Jun 1996; May - Nov 1998; Nov 1998.

4. TITLE. Enter title and subtitle with volume number and part number, if applicable. On classified documents, enter the title classification in parentheses.

5a. CONTRACT NUMBER. Enter all contract numbers as they appear in the report, e.g. F33615-86-C-5169.

5b. GRANT NUMBER. Enter all grant numbers as they appear in the report, e.g. AFOSR-82-1234.

5c. PROGRAM ELEMENT NUMBER. Enter all program element numbers as they appear in the report, e.g. 61101A.

5d. PROJECT NUMBER. Enter all project numbers as they appear in the report, e.g. 1F665702D1257; ILIR.

5e. TASK NUMBER. Enter all task numbers as they appear in the report, e.g. 05; RF0330201; T4112.

5f. WORK UNIT NUMBER. Enter all work unit numbers as they appear in the report, e.g. 001; AFAPL30480105.

6. AUTHOR(S). Enter name(s) of person(s) responsible for writing the report, performing the research, or credited with the content of the report. The form of entry is the last name, first name, middle initial, and additional qualifiers separated by commas, e.g. Smith, Richard, J, Jr.

7. PERFORMING ORGANIZATION NAME(S) AND ADDRESS(ES). Self-explanatory.

8. PERFORMING ORGANIZATION REPORT NUMBER. Enter all unique alphanumeric report numbers assigned by the performing organization, e.g. BRL-1234; AFWL-TR-85-4017-Vol-21-PT-2.

9. SPONSORING/MONITORING AGENCY NAME(S) AND ADDRESS(ES). Enter the name and address of the organization(s) financially responsible for and monitoring the work.

10. SPONSOR/MONITOR'S ACRONYM(S). Enter, if available, e.g. BRL, ARDEC, NADC.

11. SPONSOR/MONITOR'S REPORT NUMBER(S). Enter report number as assigned by the sponsoring/ monitoring agency, if available, e.g. BRL-TR-829; -215.

12. DISTRIBUTION/AVAILABILITY STATEMENT. Use agency-mandated availability statements to indicate the public availability or distribution limitations of the report. If additional limitations/ restrictions or special markings are indicated, follow agency authorization procedures, e.g. RD/FRD, PROPIN, ITAR, etc. Include copyright information.

13. SUPPLEMENTARY NOTES. Enter information not included elsewhere such as: prepared in cooperation with; translation of; report supersedes; old edition number, etc.

14. ABSTRACT. A brief (approximately 200 words) factual summary of the most significant information.

15. SUBJECT TERMS. Key words or phrases identifying major concepts in the report.

16. SECURITY CLASSIFICATION. Enter security classification in accordance with security classification regulations, e.g. U, C, S, etc. If this form contains classified information, stamp classification level on the top and bottom of this page.

17. LIMITATION OF ABSTRACT. This block must be completed to assign a distribution limitation to the abstract. Enter UU (Unclassified Unlimited) or SAR (Same as Report). An entry in this block is necessary if the abstract is to be limited.

Table of Contents

Final Technical Report

AFOSR Grant No. F49620-01-1-0474: "Surface Modification Engineered Assembly of Novel Quantum Dot Architectures for Advanced Applications" (July 1, 2001- June 30, 2007)

Program Managers: Gernot Pomrenke (AFSOR) & Dan Radack (DARPA)

P.I. Anupam Madhukar (USC); **Co-PIs**: Paul Alivisatos (UC Berkeley); Rajiv K. Kalia, Aiichiro Nakano, Priya Vashishta (USC); D. H. Rich (2001-2002); S. Chou (Princeton, 2001-2003)

I. Objectives: This DURINT (Defense University Research Initiative in Nanotechnology) sponsored research program was borne of our realization that unprecedented and novel nanosystems of importance to a wide range of applications ranging from sensors for radiation and chemical, biochemical, and biological agents to disease diagnostics and therapeutic intervention can be realized by judiciously *integrating* the continually improving power of epitaxical semiconductor nanoelectronics and nano-optoelectronics (fig 1) with the flexibility and versatility of the emerging synthetic nanocrystal-based nanostructures (quantum dots, nanorods, nanowires, etc.) (fig. 2). Such integration is captured schematically in Fig.3 and Fig. 4

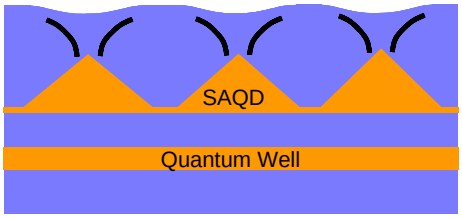

Fig.1. Schematic showing a substrate containing epitaxical quantum nanostructures (self-assembled quantum dots and quantum wells).

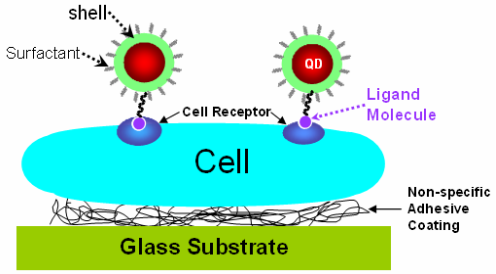

Fig.2. Schematic of the typical situation of nanocrystal QDs attached to a cell receptor (dark blue) through a ligand (purple).The live cell is typically adhered to a glass substrate through non-specific binding to a poly-peptide (commonly poly-lysine) coating on the glass.

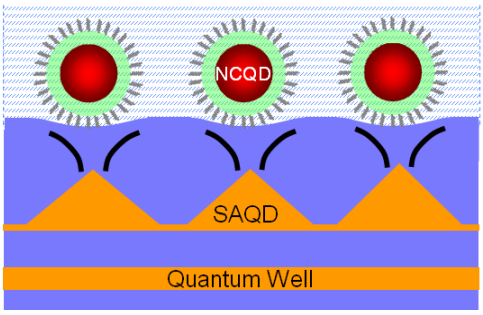

Fig. 3. A schematic showing integrated hybrid composites of *surface adsorbed* nanocrystal quantum dots (NCQDs) on chemically-modified surfaces of substrate with and without buried epitaxical quantum nanostructures.

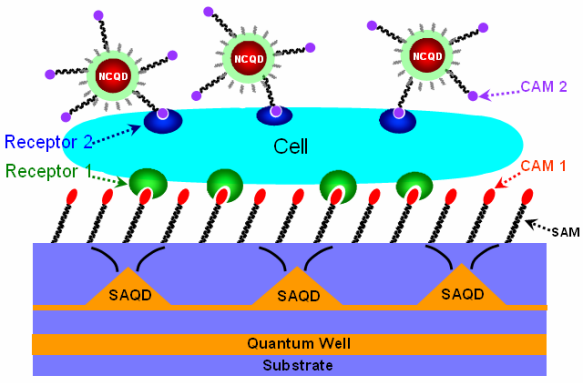

Fig. 4. A schematic showing generic scheme for biological sensing involving (a) selective adhesion of target cells on a substrate containing near-surface epitaxical quantum nanostructure; and (b) QD based cell labeling.

below. Given the usually non-overlapping synthesis and processing environments of the materials and structures for the two (the former utilizing vapor phase techniques whereas the latter typically utilizing liquid and sol-gel processes), the integration of these two classes poses complex materials and processing issues and obstacles to be overcome. Appropriate modification of the surfaces of the materials and structures involved in the two categories is the essential feature of any path towards this overall objective. Within the scope of this DURINT sponsored program (July 2001 to June 2007), this overall motivation was given concrete form through a focus on a select class of group III-V and II-VI semiconductor nanostructures and their composites but which embodied conceptual issues of generic value.

Specific objectives pursued were:

(1) Synthesis and properties (structural and optical) of integrated hybrid composites of *surface adsorbed* InAs, CdSe, PbS nanocrystal quantum dots (NCQDs) on chemically-modified GaAs surfaces with and without buried epitaxical quantum nanostructures (Madhukar);

(2) Establish methodologies for simultaneous morphological and optical examination of quantum dots on functionalized semiconductor surfaces (Rich & Madhukar)

(3) Examine nature and dynamics of charge and energy transfer between adsorbed nanocrystal quantum dots and buried near-surface quantum nanostructures (Madhukar);

(4) Examine epitaxial *overgrowth* on spherical InAs nanocrystal quantum dots adsorbed on GaAs substrate utilizing in-situ hydrogen based surface cleaning (Madhukar);

(5) Molecular dynamics simulation studies of the stress-strain distribution in systems of buried epitaxical spherical and pyramidal quantum dots (Madhukar; and Kalia, Nakano, & Vashishta);

(6) Nanoscale patterning of GaAs as templates for self-organized assembly of nanocrystals and growth of epitaxial InGaAs quantum dots (Chou, Alivisatos, Madhukar)

(7) Synthesis of II-VI branched dendrimers (tetrapods) and their electronic properties (Alivisatos);

(8) Chemical (organic self-assembled monolayer based) modification of semiconductor (Si and GaAs) and ceramic (glass, alumina) surfaces and subsequent adsorption of proteins, and peptides (cell adhesion molecules) (Madhukar);

(9) Development of inter-atomic potentials and efficient multi-length and multi-time scale algorithms for molecular dynamics simulations to examine the nature of organic SAMs and polyethelene glycol (PEG) modifying metal (Au) and semiconductor (GaAs) surfaces for adsorption of peptides / proteins (Kalia, Nakano, Vashishta),

(10) Biochemical (DNA) modification of semiconductor and metallic nanocrystals, controlled linking of such nanocrystals, and their optical response (Alivisatos);

(11) Establishing live-cell culture facilities and live-cell optical and near-field imaging (Madhukar).

II. Major Accomplishments:

In pursuing the objectives noted above, considerable new ground was broken—both conceptually and in the implementation of the ideas. Below we list the major accomplishments.

As with any study of the scope of this multi-disciplinary team effort, and one addressing such complex issues, a number of efforts were initiated and, after exploratory studies, deemed not productive or doable within the scope of the resources. The successes listed below have nevertheless benefited from such efforts not documented here. Each of the accomplishments listed below is briefly described following the list.

(1) First examinations of the structural and optical nature of colloidal nanocrystals *adsorbed on crystalline* semiconductors (Madhukar 2001-03).

(2) First investigations of the epitaxial overgrowth on semiconductor nanocrystals adsorbed on crystalline substrates, and their structural and optical properties (Madhukar 2001-03).

(3) Discovery of the inverse linear power law dependence for buried shallow pyramidal island quantum dot induced cap layer surface stress utilizing million atom molecular dynamics simulations (Madhukar 2001-02).

(4) First examination of the nature of electronic states and electron transport in tetrapods and demonstration of nanocrystal tetrapod based transistors (Alivisatos 2003-04).

(5) Development of protocols for modification of semiconductor (silicon, GaAs, alumina) surfaces with monolayer films of suitable chemical (organic SAMs) and biochemical (peptide) species, characterized for the first time on atomic scale, that perform desired function (e.g. selective cell adhesion) (Madhukar 2002-04).

(6) Development of efficient multi-length and multi-time scale algorithms for examining the nature of alkane-thiol SAMs modifying metals (Au) and semiconductors (GaAs) (Kalia, Nakano, Vashishta 2003).

(7) Use of DNA linkers for creation of controlled assemblies of nanocrystals and demonstration of plasmon-based molecular rulers (Alivisatos 2002-04).

(8) Development of inter-atomic potentials for and undertaking simulations of conjugated organic molecules (e.g. PEG) and amino acids bound to solid surfaces (Kalia, Nakano, Vashishta 2004).

(9) Demonstration of effective exciton energy transfer from nanocrystal quantum dots to adjacent buried epitaxical nanostructures such as quantum wells, a process with potential for a new paradigm for solar energy conversion (Madhukar 2005-2006).

(10) Development of methodology for hybrid quantum mechanical-classical large-scale simulations of charge/energy transfer from a localized state to substrate and demonstration through simulation of excited electron dynamics through an organic molecule-inorganic nanostructure composite (Kalia, Nakano, Vashishta 2005-06).

(11) Demonstration of colloidal synthesis of nanorod semiconductor-metal composites with predominantly single-sided metal growth and high-quality junction (Madhukar & Alivisatos 2006-07).

(12) Establishment of live-cell culture facilities and multiple-label live-cell optical and near-field imaging (Madhukar 2004-2006).

Brief Descriptions:

II. 1. Nanocrystals *adsorbed on* crystalline semiconductors (Lu, Konkar, Madhukar, Hughes, Alivisatos)

(a) Structural Properties

Publication: A. Konkar, S. Lu, A. Madhukar, S. M. Hughes, and A. P. Alivisatos, "Semiconductor nanocrystal quantum dots on single crystal semiconductor substrates: High resolution transmission electron microscopy," *Nano Lett*. **5**, 969 (2005).

A major step forward under this program was the development, for the first time, of protocols for high resolution transmission electron microscopy (HRTEM) studies of nanocrystal quantum dots on *crystalline* semiconductor substrates. All HRTEM studies of nanocrystals on solids, until the work described below, had been for amorphous substrates such as the amorphous carbon thin film in TEM grids or, a few, on polycrystalline metals.

Under this DURINT we developed procedures for thinning and ion milling GaAs(001) substrates containing MBE grown fresh epilayers to a thinness of ~20nm. An illustrative HRTEM image of such a membrane substrate is shown in Fig.1.1 below. The lattice fringes in the image correspond to the orthogonal <220> GaAs planes. The spacing between the planes is 0.2 nm. In-situ atomic force microscope (AFM) imaging of the as-grown samples showed that the typical surface consists of ~ 200 nm wide (001) terraces separated by monolayer high steps.

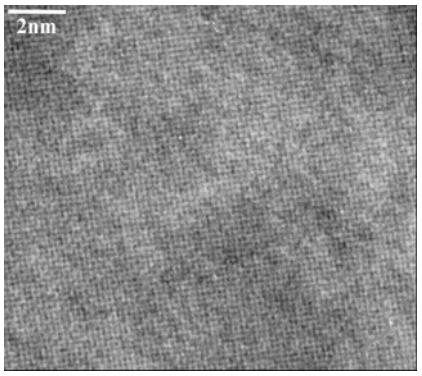

Fig 1.1. Illustrative HRTEM image of as-prepared GaAs ultra-thin membrane

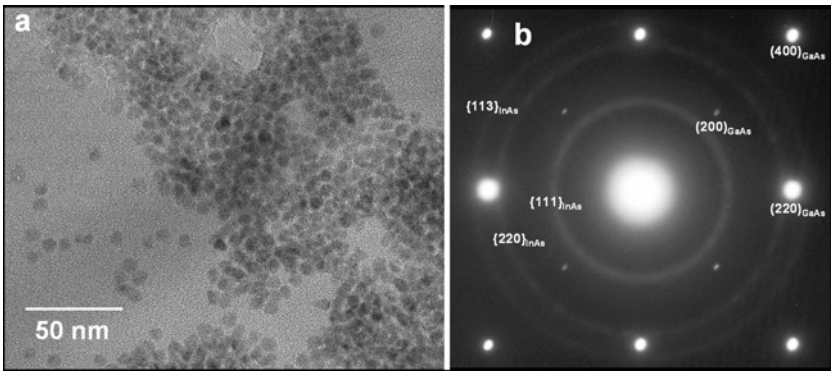

Fig 1.2(a) Low magnification TEM image of InAs NCQDs on an ultra-thin GaAs membrane. (b) Corresponding selected area diffraction pattern.

Protocols for the controlled deposition of the nanocrystals on such membranes were established. In particular, the nature of the interface between the trioctylphosphine(TOP) surfactant covered InAs nanocrystals and the GaAs(001) membrane substrate was examined. Figure 1.2(a) shows a low magnification image of the InAs nanocrystal quantum dots (NCQDs) on an ultra-thin GaAs membrane. Due to the small dispersion in their sizes the NCs are seen to form large patches of hexagonally close packed monolayer structures. In addition, small patches composed of few to tens of NCQDs and isolated NCQDs are also observed. The NCQDs have a nearly spherical shape and an average diameter of ~ 8 nm. A selected area diffraction pattern is shown in Fig.1.2(b). The bright spots originate from electron diffraction from the GaAs substrate and the superimposed rings from the InAs NCQDs. The intensity of the rings is uniform along

their circumference indicating that the NCQDs do not have a preferred orientation on such atomically flat substrates. This lack of preferred orientation might be due to the TOP molecules covering the NC surface. Another possibility is that the NCs do not have sizeable well defined facets.

Figure 1.3 shows HRTEM image of a single isolated InAs NCQD. Well defined lattice fringes from both the NCQD (spacing 0.35 nm) and GaAs substrate (spacing 0.2 nm) are seen in the image. The contrast in the image can be qualitatively understood as resulting from two independent interference effects: the forward scattered beam and (a) the {111} InAs diffracted beam from the NCQD or (b) the {220} GaAs diffracted beam from the GaAs substrate. A dark halo surrounding the NC is also observed. The width of the halo is ~ 1 to 1.5 nm. The origin of this contrast is not certain. However, as the length of TOP from the P atom to the 3 terminal C atoms is ~ 1.3 nm, we speculate that the layer of TOP molecules surrounding the NC is likely responsible. If true, this will be consistent with the observed lack of preferred NC orientation, as noted above. The TOP layer may be able to effectively screen the otherwise expected covalent interaction between the NC atoms and the GaAs substrate.

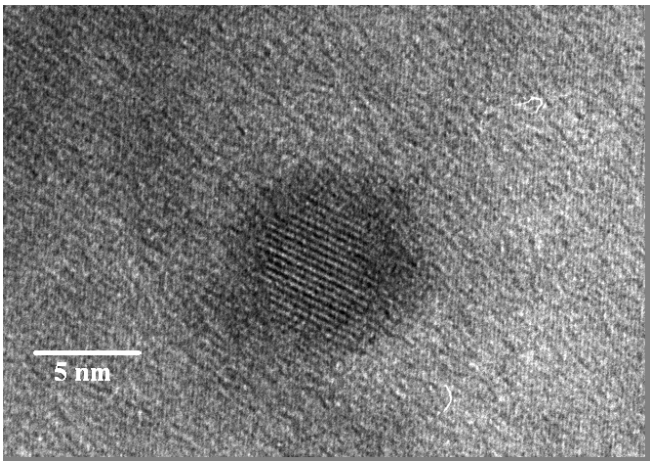

Fig 1.3. HRTEM image of a single isolated InAs NCQD on GaAs(001). Note the {111} InAs lattice fringes within- and the dark halo around the NCQD.

The impact of longer exposure of the nanocrystal to the electron beam, i.e. radiation damage effect, was also examined. It was found that long exposures can, in fact, even convert InAs nanocrystals into essentially In clusters. Thus reliable structural studies of these delicate systems require special care.

(b) Optical Behavior of Adsorbed InAs/ZnSe Core-Shell Quantum Dots

Another ground-breaking effort under this program was the first examination of the optical response of semiconductor nanocrystal quantum dots on *crystalline* semiconductor substrates with and without buried epitaxical nanostructures and the demonstration of energy transfer *from* the NCQDs *to* the underlying confined quantum structure. For the first optical studies of hybrid NCQD-semiconductor systems, focus was on the InAs/ZnSe core-shell NCQDs. These NCQDs were dispersed, at varying densities, on sulfur-passivated GaAs(001) substrates. The surface density, and the fact that the morphology was maintained as a single layer of NCQDs, was ascertained from systematic AFM studies. In fig.1.4 we show the photoluminescence (PL) behavior of the InAs/ZnSe TOP covered NCQDs in solution and when placed on glass substrate. The band gap of the glass being very large (>5eV) compared to the

fundamental transitions in the NCQDs and the GaAs/InGaAs based quantum nanostructures, it acts as a meaningful reference for examining the impact on the PL efficiency when the NCQDs are dispersed on the GaAs semiconductor substrates.

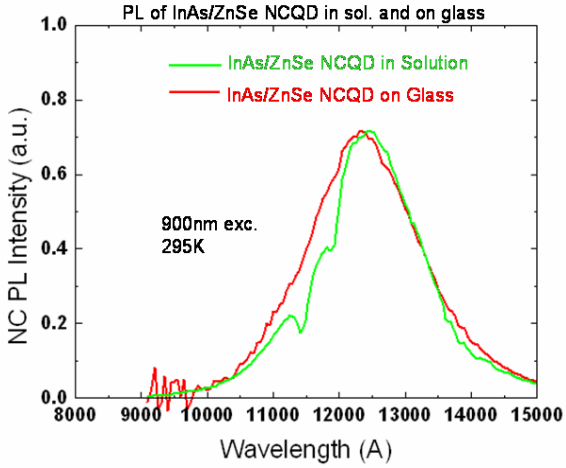

Fig 1.4. Room temperature photoluminescence behavior of InAs/ZnSe core/shell nanocrystals in solution(Green) and on glass substrate.

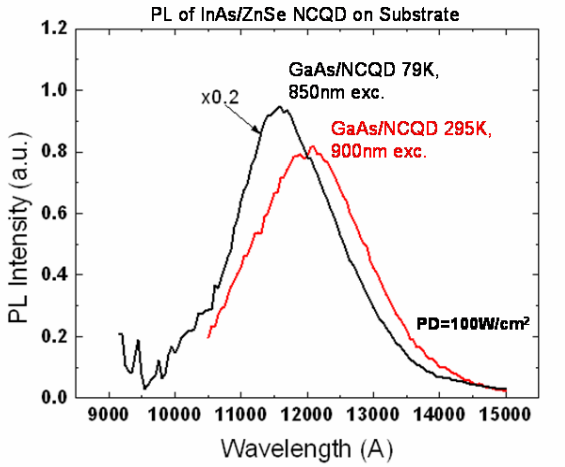

Fig 1.5. Photoluminescence behavior of InAs/ZnSe core/shell NCQD on sulfur-passivated GaAs substrate at 79K(black) and at 295K(red)

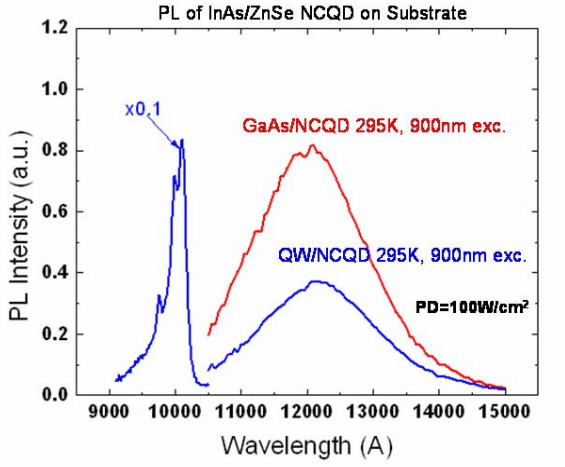

Fig 1.6. Room temperature photoluminescence of InAs/ZnSe core/shell NCQD dispersed on GaAs (red) and GaAs substrate containing an InGaAs quantum well buried about 5nm below the surface (blue). In both cases the GaAs surfaces are sulfur-passivated

The excitation energy and power dependence of the NCQD-semiconductor hybrid systems as a function of temperature were systematically examined. In figure 1.5 is shown an

illustrative PL spectra from the InAs/ZnSe NCQDs dispersed over GaAs(001) substrate. Note the expected shift in the PL peak with increasing temperature and the reduction in the intensity due to shortening of the exciton life-time. In fig.1.6 is shown the room temperature PL behavior for the NCQDs on the GaAs substrate (same as fig.1.5) and on a GaAs substrate containing an InGaAs quantum well buried about 5nm below. Note the drop in the NCQD PL intensity, clearly indicating a transfer of energy to the quantum well. *This was the first observation of energy transfer between nanostructures belonging to two entirely different classes:* one, the nanocrystal quantum structures, suited for biochemical/biological applications in solution environments and the other, the epitaxical semiconductor quantum structures, which are the essence of all current advanced electronic and optoelectronic semiconductor technology. Our results lay the first stepping stones towards development of exciting and potentially revolutionary technologies with applications ranging from communications to solar energy conversion (see item 10 below) to information sensing and processing in biomedical environments.

II. 2. Epitaxical Overgrowth on Nanocrystals (Lu, Konkar, McCabe, Ho, Zhang, Chen, and Madhukar)

Publication: A. Madhukar, S. Lu, A. Konkar, Y. Zhang, M. Ho, S. Hughes, and A. P. Alivisatos, "Integrated Semiconductor Nanocrystal and Epitaxical Nanostructure Systems: Structural and Optical Behavior," *Nano Lett.* **5**, 479 (2005).

An objective of this program was to explore the integration of nanocrystals (NCs) with vapor phase grown solid state nanostructures (such as quantum wells, wires, and the self-assembled island quantum dots) to create composite structures with new and novel functionalities. A fundamental challenge here is discovering procedures that take NCs residing in a solution (non-aqueous or aqueous) environment, depositing them on semiconductor substrate in a controlled and reproducible fashion, and then recovering from the chemical contamination resulting from the process. (Note that even high purity chemical reagents used in colloidal synthesis etc. are enormously dirty by the standards of semiconductor electronic grade materials). As if overcoming the chemical contamination problem were not challenging enough, increasing thermodynamic instability and evaporation rate of nanocrystals with decreasing radius places severe constraints on the window of parameters within which acceptable cleaning must be realized without significant structural changes in the NCs and the semiconductor substrate.

The second fundamental challenge to be faced once the first is overcome is the overgrowth of appropriate capping layer for the NCs on the cleaned semiconductor substrate with sufficiently low structural and chemical defects. Once again the parameter ranges for the growth are very restrictive as the original nanocrystal cannot be allowed to essentially lose their structural identity during the procedures leading to capping.

(a) InAs NC adsorption on GaAs and Impact of H-Cleaning (Chen, Ho, Zhang, and Madhukar):

Substantial progress was made in addressing both the above noted challenges. Indeed, since the usually employed approach of high temperature thermal de-oxidation of the native oxide, left behind on a semiconductor surface at the end of solution based chemical cleaning procedures, cannot be carried out with the NCs adsorbed, we needed to find a low temperature but efficient cleaning procedure. To this end, we designed, acquired, installed, tested, and employed an ultra high vacuum (UHV) H radical cleaning system in a chamber that is UHV inter-connected to the MBE growth chamber. To separately address the issue of the true nature of

the GaAs surface on which the InAs NCs are deposited, we used GaAs substrates with freshly MBE grown GaAs or InGaAs epilayers. Such substrates are brought from the MBE growth chamber to a glove box attached to the MBE system in which an inert atmosphere is maintained by continuous flow of ultra high purity Ar gas. In this glove box the InAs NCs are deposited from the solution and wick-dried, all within a couple of minutes and the sample re-inserted into the UHV environment where it is degassed before insertion into the H-cleaning chamber.

(b) Adsorbed NC Density Control:

To establish reproducible adsorption densities, a systematic study utilizing ex-situ AFM determination of NC density and surface morphology was undertaken as a function of the dilution with respect to the stock solution calibrated against optical density. Figure 2.1 (panels a through e) show some typical AFM images for 5 second depositions from solutions of the marked dilutions. The corresponding AFM determined surface densities are plotted in fig. 2.2.

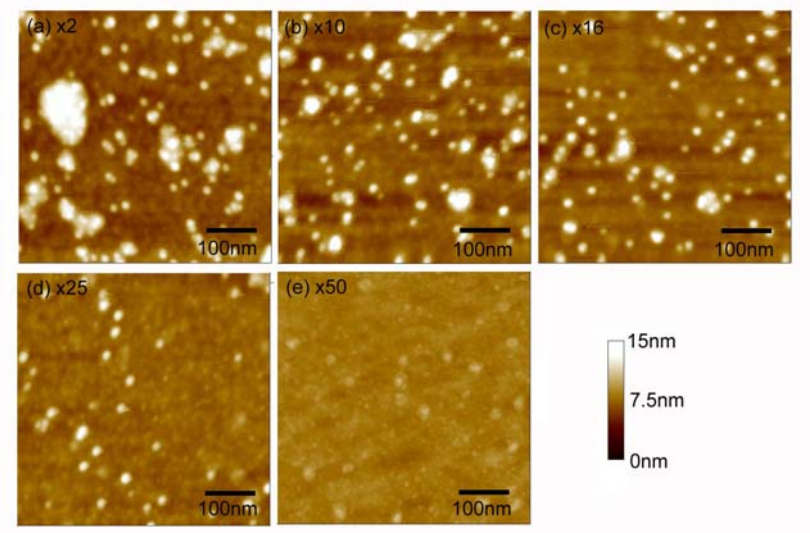

Fig 2.1. AFM image of as-deposited InAs NC on GaAs (5 sec deposition from marked dilutions)

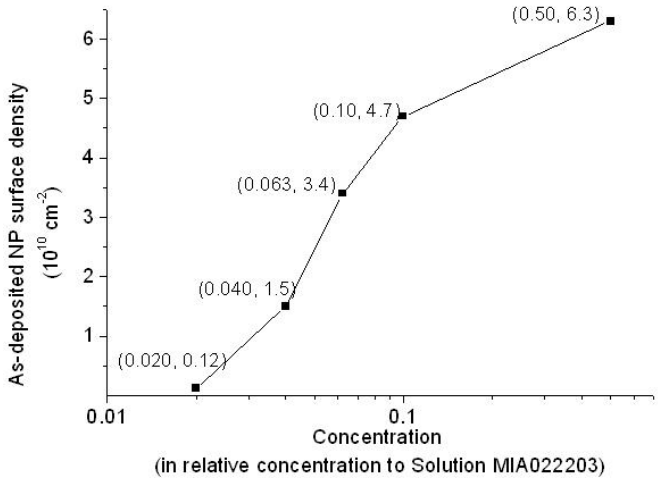

Fig 2.2. InAs NC surface density as deposited vs. solution concentration.

(c) Impact of H cleaning conditions on InAs NCs:

The degree of chemical cleaning necessary for high quality response from the overgrown capping layer was established by mounting two substrates side-by-side, one with the NCs as noted above and another without the NCs but exposed only to the toluene solution (in which the NCs are otherwise dispersed). Separately, freshly grown GaAs epilayer exposed only to the glove box environment were also H cleaned in the same range of conditions as explored so far for the NC deposited samples. On all such pairs and triplets of samples cleaned with H, ex-situ AFM was carried out to determine the degree of change in the size distribution of the NCs and the nature of the surface roughness.

In fig.2.3, panels (a) through (d), are shown illustrative AFM images of InAs NC/GaAs samples with starting density of ~$6x10^{10}$ per cm^2 cleaned at the temperature and time combinations indicated. Note that at the lower temperatures (~200℃/1hr) the nanocrystal density and average size remain the essentially the same as the as-deposited values whereas at the higher temperature and time combination (410℃/1hr or 350℃/2hrs), the density and the average size are reduced to approximately half. Finally, panel d of fig. 4 shows that after 1hour of annealing, following the cleaning at 410℃ for 1hr, the NC density is over an order of magnitude reduced and the average size is only ~2nm. We believe the NCs are in part evaporated and in part interdiffused with the GaAs substrates at these high temperatures. These results indicate the difficulty in finding the temperature/time window such that adequate chemical cleaning is achieved but without significantly compromising the size and nature of the NCs. Figure 2.4 shows the behavior of the NC density versus size for H cleaning conditions corresponding to the four panels of fig. 2.3.

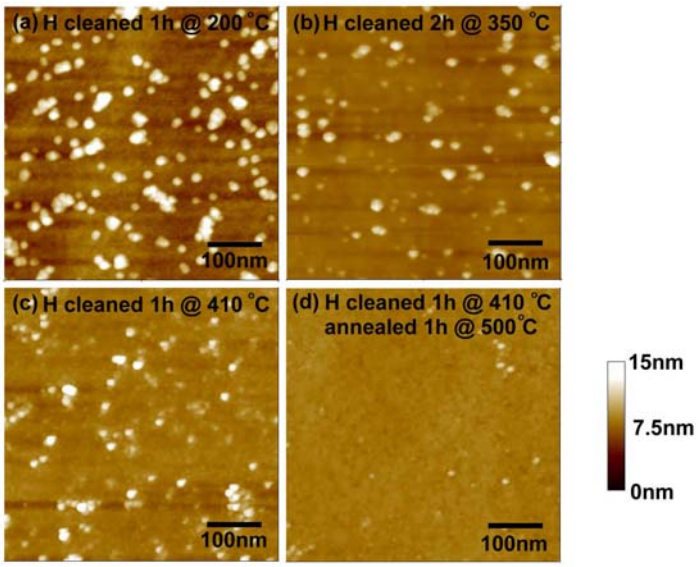

Fig. 2.3. AFM image shows InAs NC size reduction due to H-cleaning

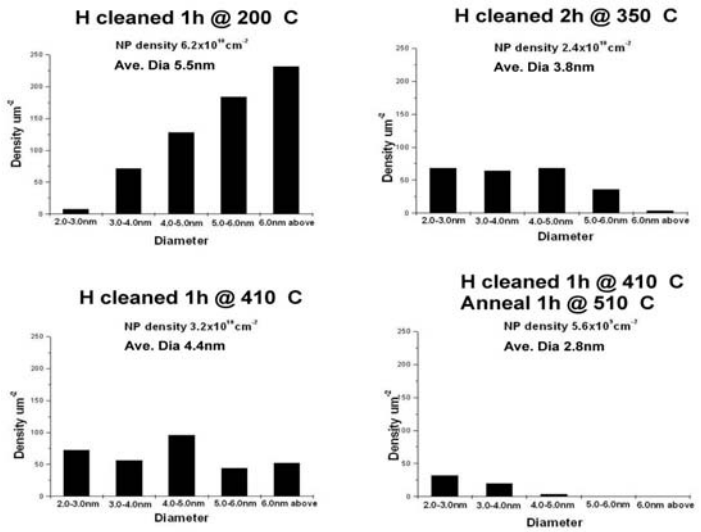

Fig 2.4. InAs NC sized distribution vs. H-cleaning condition

(d) Overgrowth of GaAs capping layers on H-cleaned InAs NCs (USC):

For each H cleaning case discussed in the preceding section, two corresponding samples (with and without the NCs) were H-cleaned and inserted back into the MBE chamber and GaAs overlayer grown to examine the photoluminescence (PL) of the resulting ideal structure (see schematic of fig .2.5). In some cases a one monolayer of InAs was grown first to mimic the wetting layer known to form in the case of InAs/GaAs self-assembled epitaxical island quantum dots. This serves as a built-in optical marker of the nature and quality of the overgrowth.

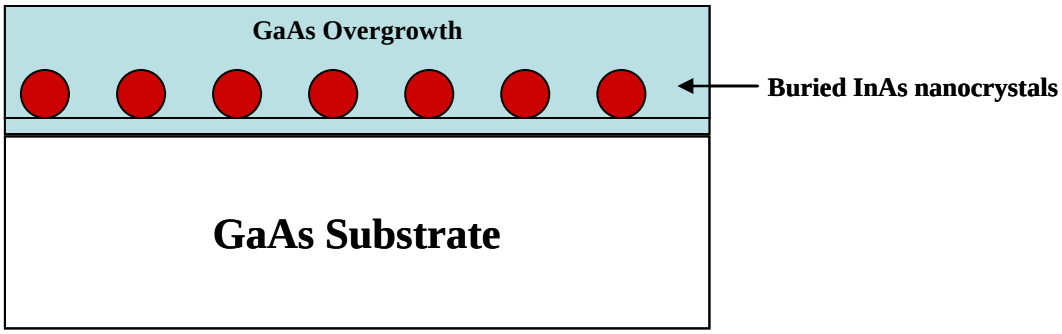

Fig. 2.5. Schematic showing overgrowth on nanocrystals adsorbed on a substrate.

Figure 2.6 shows the PL behavior of the samples for GaAs exposed to the glove box environment, to toluene, and to NCs, all subsequently cleaned at 410°C for 1 hour, and all overgrown with 170ML of GaAs via migration enhanced epitaxy at 300°C. The PL from GaAs is seen in all cases at ~819nm (from recombination of free or bound excitons) and at ~835nm (from recombination involving electron and carbon acceptor level). In the case of the NCs, a 1ML InAs was deposited and the corresponding PL at ~851nm (1.457eV) is seen. This suggested that the H cleaning of the system is of sufficient quality to allow emission from the grown overlayers. Although no clear peak evidencing the presence of the original NCs is seen, enhanced emission

in the long wavelength tail region (shoulder marked by the black arrow) is seen. The enhanced tail emission is consistent with expected emission wavelength from the reduced sizes of ~2nm of the remnant InAs nanocrystals after the H cleaning at 410°C as noted above.

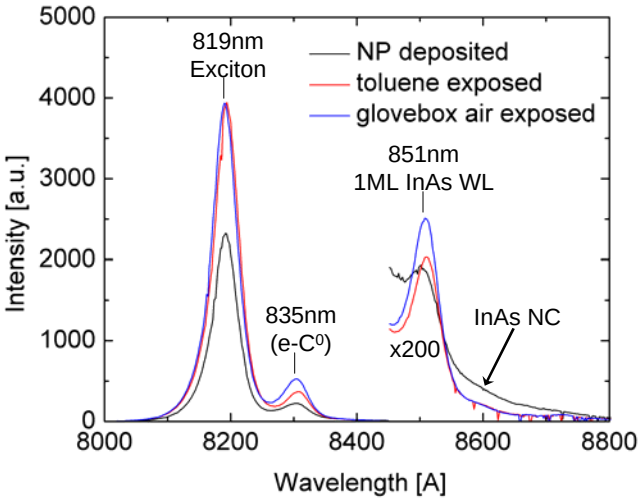

Fig 2.6. Photoluminescence of GaAs exposed to glovebox environment, toluene, and to InAs NC, H-cleaned at 410 ^{o}C for 1hour and overgrown with 170ML GaAs via MEE epitaxy. Ar^{+} 514nm excitation @ 6K.

An independent test of the situation is, of course, the ability to resolve structural features in high resolution TEM. Within the capabilities of the microscope available for these studies, 1-2nm buried In-rich regions (due to intermixing of In and Ga) would not be resolvable. Importantly, the structural images did not reveal significant density of extended defects (dislocations, stacking faults, twins) in the overgrowths for systems cleaned at 410C as exemplified in the typical cross sectional TEM image shown in fig.2.7. This is encouraging as it suggests that the remaining difficulty to be overcome is only the controlled reduction of the as-deposited NC size to a remnant size commensurate with desired response wavelength which can be helped enormously by synthesizing and thus starting with larger average size NCs.

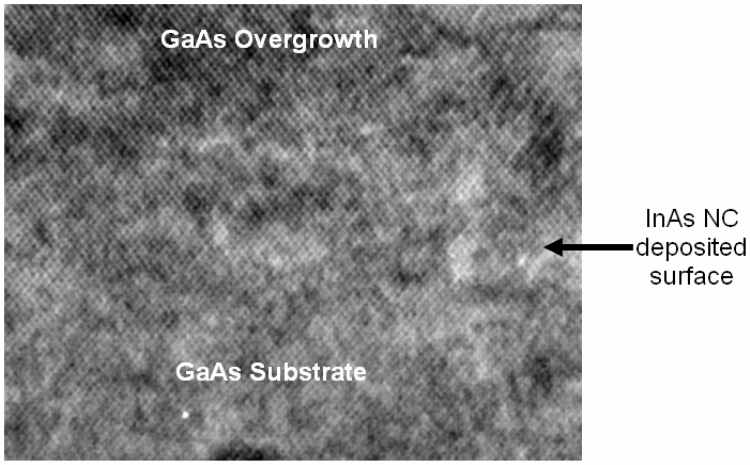

Fig 2.7. TEM lattice image showing defect free overgrowth on InAs NCs

.

II. 3. Strain Distribution due to Pyramidal Island Quantum Dots

(a) Discovery of Inverse Linear Dependence of Shallow Pyramidal Quantum Dots Induced Strain Field (Makeev and Madhukar)

Publications:

M. A. Makeev and A. Madhukar, "Simulations of atomic level stresses in systems of buried Ge/Si islands", *Phys. Rev. Lett.* **86**, 5542 (2001).

M. A. Makeev and A. Madhukar, "Stress and strain fields from an array of spherical inclusions in semi-infinite elastic media: Ge nanoinclusions in Si," *Phys. Rev. B* **67**, 073201 (2003).

M. A. Makeev, W. Yu, and A. Madhukar, "Stress distributions and energetics in the laterally ordered systems of buried pyramidal Ge/Si(001) islands: An atomistic simulation study," *Phys. Rev. B* **68**, 195301 (2003).

A central aspect of the DURINT efforts was to synthesize vertically self-organized buried epitaxical island QDs and the nanocrystal QDs on the surface of the capping layer burying the island QDs. The vertical self organization, as the Madhukar group first demonstrated experimentally and theoretically (Xie et al., Phys. Rev. Letts., 75, 2542 (1995)) exploits the stress induced by the buried islands at the capping layer surface to induce directed surface diffusion of the incoming adatoms towards regions of tensile strain above the apices of the buried islands.

That lattice mismatched inclusions create stress fields in the surrounding solid medium is a well studied phenomena, the simplest case of a spherical inclusion being a well known text book example. Linear elasticity theory gives the far-field stress behavior as depending on the inverse cubic power of the distance from the center of the spherical inclusion. This simple model was employed by us in providing the first model and theory (see the ref. noted above) for vertical self-organization during growth on a surface with buried inclusions, such as the self-assembled 3D pyramidal island quantum dots formed in highly latticed mismatched systems such as InAs/GaAs and Ge/Si. However, the shape of these islands being pyramidal, and the sizes being nanoscale, it was an important issue to assess the quantitative reliability of the simple spherical inclusion model to this technologically important class of quantum dots. To address this, molecular dynamics simulations of the stress induced by pyramidal shallow islands were undertaken. A schematic of the simulation system is shown in Fig.3.1. The system chosen was Ge-Si since well-tested interatomic potentials already existed for this system. The finding of the

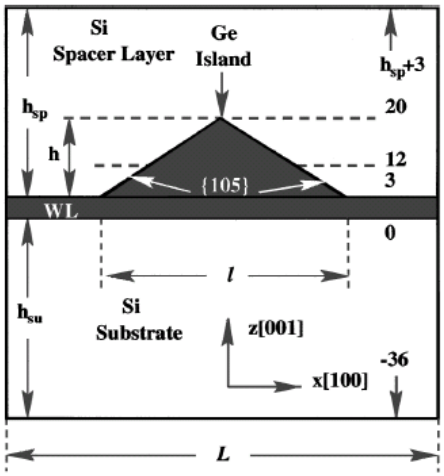

Fig. 3.1. Schematic illustrating the modeled system. Germanium island of height h (with WL of 3 ML underneath) is positioned on a Si(001) substrate of thickness h_{su} and covered by Si(001) spacer layer of thickness h_{sp}. The lateral size of the simulation box, $L = 60a_{Si}$, and the lateral island size is 1. Here a_{Si} is the lattice constant of Si, a_{Si} =5.430 95 Å. Numbers correspond to the atomic planes z coordinate, measured in ML, N_z .

simulations for the stress at and near the surface of the layer burying the islands (called the spacer layer) as a function of its thickness (h_{sp}) is shown in Fig.3.2. Unlike the inverse cubic dependence on the distance for the spherical inclusion, we found that the stress at the surface directly above the island apex decays much slower with *an inverse power dependence*. This has considerable significance for the design of self-assembled island quantum dots based devices (lasers, detectors, etc.). It also drew attention to the potential significance of the shape of the inclusion in controlling the nature of the stress distribution. Indeed, following this discovery, we carried out simulations with steep pyramidal islands and found the stress dependence to be closer to the inverse cubic power law. Indeed, the strength of the stress at the point above the apex was found to depend upon the surface area of the island for the shallow island but the volume for the steep island, thus indicating a change in the behavior as essentially a change in the effective dimensionality of the island as it goes from shallow to steep.

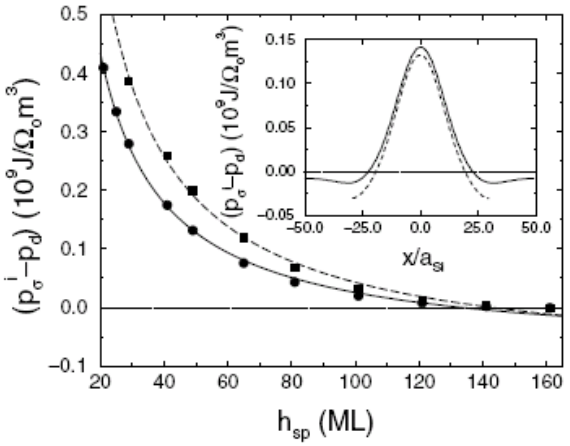

Fig. 3.2. Normalized hydrostatic stress on the spacer surface (circles) and 5 ML below (squares) at the point above the island's apex, plotted as a function of spacer layer thicknesses, h_{sp}, measured in ML. Solid line shows a fit that gives $p^i_s(h_{sp}) - p_d = -0.07 + 10.21/h_{sp}$. Long-dashed line approximates the stress measured 5 ML below the spacer surface. Inset shows the x dependence of the hydrostatic stress for simulation cell sizes $L = 100a_{Si}$ (solid line) and $L = 60a_{Si}$ (dashed line), with $h_{sp} = 49$ ML.

(b) Parallel Molecular Dynamics Simulations of Steep Pyramidal InAs/GaAs Quantum Dots: (Makeev, Nakano, Kalia, Vashishta, and Madhukar)

To gain a more quantitative understanding of the strain distribution for the InAs/GaAs pyramidal island quantum dot systems, we applied molecular dynamics techniques on massively parallel computing platforms to simulate the stress distributions due to InAs pyramidal islands buried in GaAs matrix at varying depths. This was made possible by the development and testing (in the first two years of the DURINT effort) of reliable inter-atomic potentials for In, Ga, and As atoms in differing environments, including the mixed configurations involved at interfaces. The results obtained for the InAs/GaAs pyramidal islands supplement and complement our simulation results obtained and noted above for the Ge pyramidal islands buried in Si matrix.

A schematic illustration of the model InAs/GaAs system is shown in Fig.3.3. The simulation cell consists of a GaAs substrate with vertical size of $60\mathbf{a}_{GaAs}$, where $\mathbf{a}_{GaAs}$ is the lattice constant of GaAs ($\mathbf{a}_{GaAs} \approx 5.63$ A). The lateral sizes of the simulation system, in both x- and y-directions, are $200a_{GaAs}$ (~ 112 nm). A {101}-facetted InAs island, with lateral dimensions of ~ $60\mathbf{a}_{GaAs}$, is positioned on the GaAs substrate, with 1 double layer of InAs WL beneath, and covered with GaAs spacer layers of varied thickness from ~5 nm to ~ 20 nm.

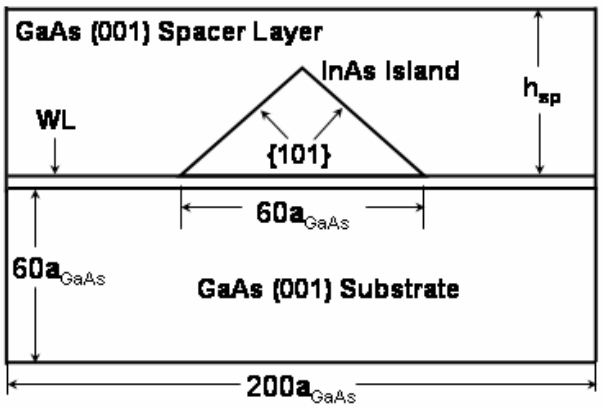

Fig 3.3. Schematic of simulated InAs/GaAs model system

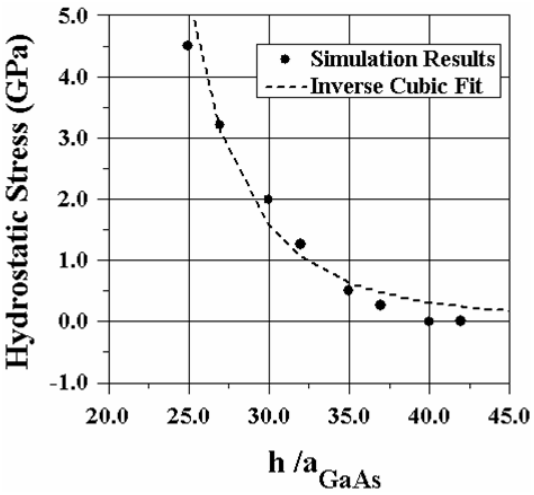

Fig. 3.4. Simulated InAs pyramidal QD spacer layer surface hydrostatic stress dependence on the spacer layer thickness, h_{sp} (solid dots) along with $\sim 1/h_{sp}^3$ fit (dashed line).

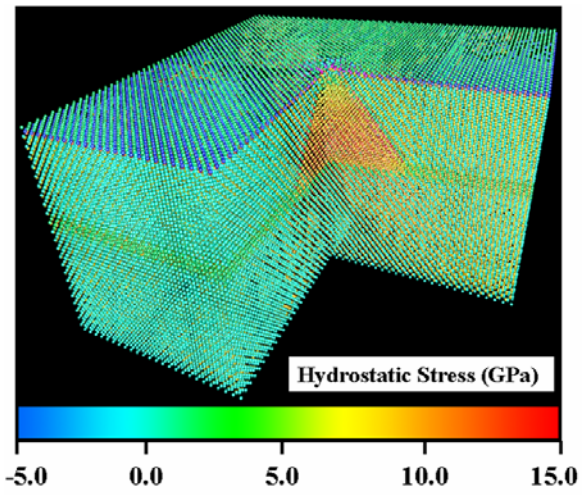

Fig. 3.5. Hydrostatic stress distribution in and around the InAs pyramidal island QD buried in GaAs matrix.

The computed spacer layer surface hydrostatic stress dependence on the spacer layer thickness, h_{sp} is shown in Fig. 3.4 (solid circles), along with $\sim 1/h_{sp}^3$ fit (dashed line). The obtained fit is quite adequate in describing the hydrostatic stress behavior for small and intermediate values of the spacer layer thickness. The inverse cubic dependence found for the steep {110} side wall InAs/GaAs pyramidal islands is different from our finding of an inverse dependence for shallow pyramidal island quantum dots and indeed, is closer to the historical inverse cubic dependence found analytically for spherical objects buried in an elastic medium. Clearly, symmetry of the buried object impacts whether, to the leading order, a dipole approximation for the buried object is adequate for describing elastic fields.

To obtain a complete picture of the stress behavior in the InAs/GaAs QD systems, the hydrostatic stress distributions in and around the buried InAs pyramidal island QD in the GaAs

matrix were examined. An example of the stress distribution is shown in Fig.3.5 in the form of a color-coded map. As expected, compressive hydrostatic stress, observed in the island's interior, relaxes towards the island apex from the bottom of the island, and falls off in the lateral direction as distance from the island center increases. The stress turns tensile in the region above the island and near the GaAs over-layer surface, with a region of tensile stress above the island apex observed.

II. 4. Tetrapods: Electronic Nature and Transistors (A. P. Alivisatos)

Publications:

L. Manna, E.C. Scher, and A.P. Alivisatos, "Shape Control of Colloidal Semiconductor Nanocrystals," *Cluster Sci.* 13, 521(2002).

L. Manna, D.J. Milliron, A. Meisel, E.C. Scher, and A.P. Alivisatos, "Controlled Growth of Tetrapod-Branched Inorganic Nanocrystals," *Nature Mat.*, **2**, 382-385 (2003).

Y. Cui, U. Banin, M. T. Bjork, and A. P. Alivisatos, "Electrical transport through a single nanoscale semiconductor branch point," *Nano Letters* **5**, 1519 (2005).

(a) II-VI Tetrapod Synthesis and Properites

At Berkeley, a method was developed for creating colloidal II-VI branched semiconductor "tetrapods. In fig.4.1, panel (a), are shown the absorption spectra of three different tetrapods, all having the same arm lengths but different size quantum dot at the junction. Note the shift in the absorption peak, demonstrating that the absorption is due to the quantum dot. In panel (b) we show the absorption behavior when the quantum dot size is held fixed and the arm lengths are allowed to vary. Note that the absorption peak remains fixed, demonstrating, once again, that the dominant absorption is in the quantum dot.

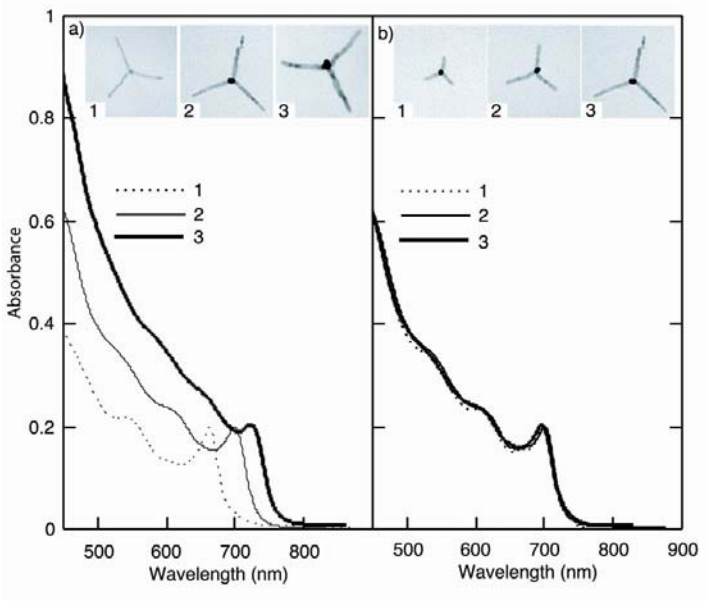

Fig 4.1. (a) Absorption spectra of tetrapods of same arm length but different quantum dot size at the junction, as shown in the inset. (b) Absorption spectra of tetrapods of different arm length but same quantum dot size at the junction, as shown in the inset.

Such a coupled quantum dot-quantum wire structure, i.e. a tetrapod, was utilized for the first time to create single electron transistors, as discussed below.

(b) Tetrapod Single Electron Transistors (A. P. Alivisatos et al.)

To carry out electrical studies of branched tetrapods, under this program we developed the capability to attach electrodes to the three arms of a tetrapod that lie on a surface (the fourth arm is sticking up) as shown in Fig. 4.2. Because the electrical characteristics of the tetrapod will be dominated by the junction point, this allows us to readily create electrical contacts to extremely small nanocrystals (as small as 2nm).

Mono-disperse CdTe tetrapods with arms 8 nm in diameter and 150 nm in length were synthesized. The tetrapods dispersed in toluene were deposited onto ~10 nm thick Si_3N_4 dielectrics with pre-patterned alignment markers on the top and a conducting substrate back gate underneath. [24] When a tetrapod is placed on a solid substrate, it spontaneously orients with one arm pointing perpendicularly away from the substrate and three arms projecting down towards the surface. Electron-beam lithography is used to place individual 60 nm-thick Pd electrodes to each of the three arms that point downwards so that there are a total of four terminals (three arms and a back gate) in the devices as shown schematically in Fig.4.2 top inset. Figure 4.2 bottom inset shows a typical scanning electron microscopy image on a tetrapod contacted with three 100 nm-wide electrodes. The center brighter spot is due to the fourth arm pointing up away from the substrate although some devices lost this arm during the lift-off process. The separation between the metal electrodes and the tetrapod junction point ranges from 30 to 80 nm in all of the devices. The devices were loaded into a Helium-flow cryostat for low-temperature electrical measurements.

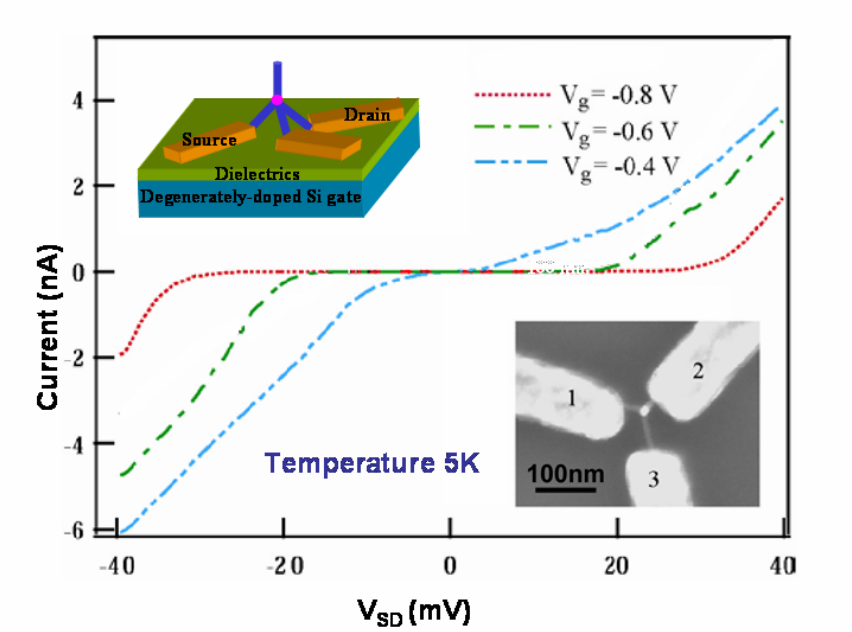

Fig 4.2. Typical I-V_{SD} curve of a tetrapod single electron transistor at different back gate voltage (V_g) while the third arm is floating. (Top inset: Schematic of a tetrapod single electron transistor. Bottom inset: SEM image of such a tetrapod single electron transistor.)

Typical curves of current (I) as a function of source-drain bias voltage (V) through arm pair 1-2 (Fig.4.2 bottom inset) at different back gate voltage (V_g) while keeping the third arm floating are presented in Fig.4.2 main panel. The I-V curves show a strongly suppressed conductance at small V and step-like increase of current at high V, suggesting single electron charging behavior. The size of the zero conductance gaps could be changed reversibly by V_g and the gap could be completely closed by changing V_g. The measurements through pair 2-3 and 1-3 show similar behavior. More than 20 working devices fabricated from 5 different independent processes were measured.

It was found that the electrical transport characteristics of these transistors fall into two different categories. Systematic examination of the I-V characteristics as a function of the gate bias and temperature reveals that these two classes represent tetrapod structures having different strengths of coupling between the dot and rod regions and thereby causing differing electron transport mechanisms involving incoherent or coherent transport.

II. 5. Semiconductor and Ceramic Surface Modification by Organic SAMs and Peptides (Lu, Bansal and Madhukar)

Publication:
S. Lu, A. Bansal, W. Soussou, T. W. Berger, and A. Madhukar, Receptor-ligand based specific cell adhesion on solid surfaces: hippocampal neuronal cells on bilinker functionalized glass, Nano Lett. **6**, 1977 (2006).

The capability to control the surface property of a substrate or a solid-state device is the critical foundation on which is built the theme of research pursued under this DURINT program. The surface properties of the substrate are at the heart of the controlled adsorption of nanoscale objects (nanocrystals, peptides, proteins, cells) in random or ordered arrays. For chip based sensitive biological detection, the surface property of the chip controls the electrical or mechanical coupling between the adsorbed biological entities (proteins, cells) and the underlying solid state devices.

The generic strategy employed is to modify the surface properties of a solid via functionalizing it with a chemisorbed layer of designed organic (including bioorganic) molecules. Such molecules typically consist of a hydrocarbon chain (often alkyl chain) which, at the substrate end, has a functional group to bind to the surface atoms and, at the free end, an appropriate functional group to serve the desired purpose of surface modification. Such a functional group at the free end may be as simple as a single atom that enables the attachment of a QD or as complicated as an oligopeptide for the attachment a specific antigen or live cell.

The chemisorbed molecules on the surface often assemble into a closely packed monolayer referred to as a self assembled monolayer (SAM). The SAM is a powerful tool for surface modification given its great design flexibility: thickness and electronic property of SAM can be tuned with the appropriate hydrocarbon chain length and structure; the functional group needed to bind at the solid substrate; and the free end can be chosen to be a chemical group or biochemical molecule according to the entity to be attached, such antigens or cells.

Under this program, semiconductor and ceramic surface modification using SAMs based on (a) organic hydrocarbon molecules and (b) bioorganic oligopeptide molecules were investigated for a range of purposes, as briefly documented below.

(a) Organic SAMs:

We developed protocols for uniform and dense adsorption of hydrocarbon based self-assembled monolayer (SAM) on semiconductor/ceramic surface. The typical functional groups used in our work for anchoring the SAM onto surface are: silane group for Si/SiO_2 (or glass), thiol group for GaAs, carboxylic group for alumina. The conditions and procedures to achieve high quality SAM adsorption were obtained using feedback from atomic force microscope (AFM) imaging. Systematic AFM studies are carried out to examine GaAs, Si/SiO2, glass, and alumina substrates for their starting topology (roughness) prior to surface modification as well as their behavior after coating with SAM.

Figure 5.1 shows four illustrative examples of AFM images of SAM modified Silicon and GaAs surfaces. The quality of the SAM coating is evident from the small roughness of the surfaces after SAM modification (compared to the length of the SAM molecules). Specifically, octadecyl-tricholorosiloxane (ODS) (Fig 5.1a) and octadecanethiol (ODT) (Fig 5.1c) with methyl group as the free end are used to modify, respectively, silicon and GaAs surface to endow hydrophobicity to the surface for enhanced non-specific protein adsorption. 3-bromopropyl-tricholoro-silane (BPTS) with bromine group as the free end (Fig 5.1b) and 1,6-hexanedithiol with thiol group as the free end (Fig 5.1d) are used to modify, respectively, silicon and GaAs surface for specific binding to thiol groups on protein surfaces such as those contained in the cysteine amino acids.

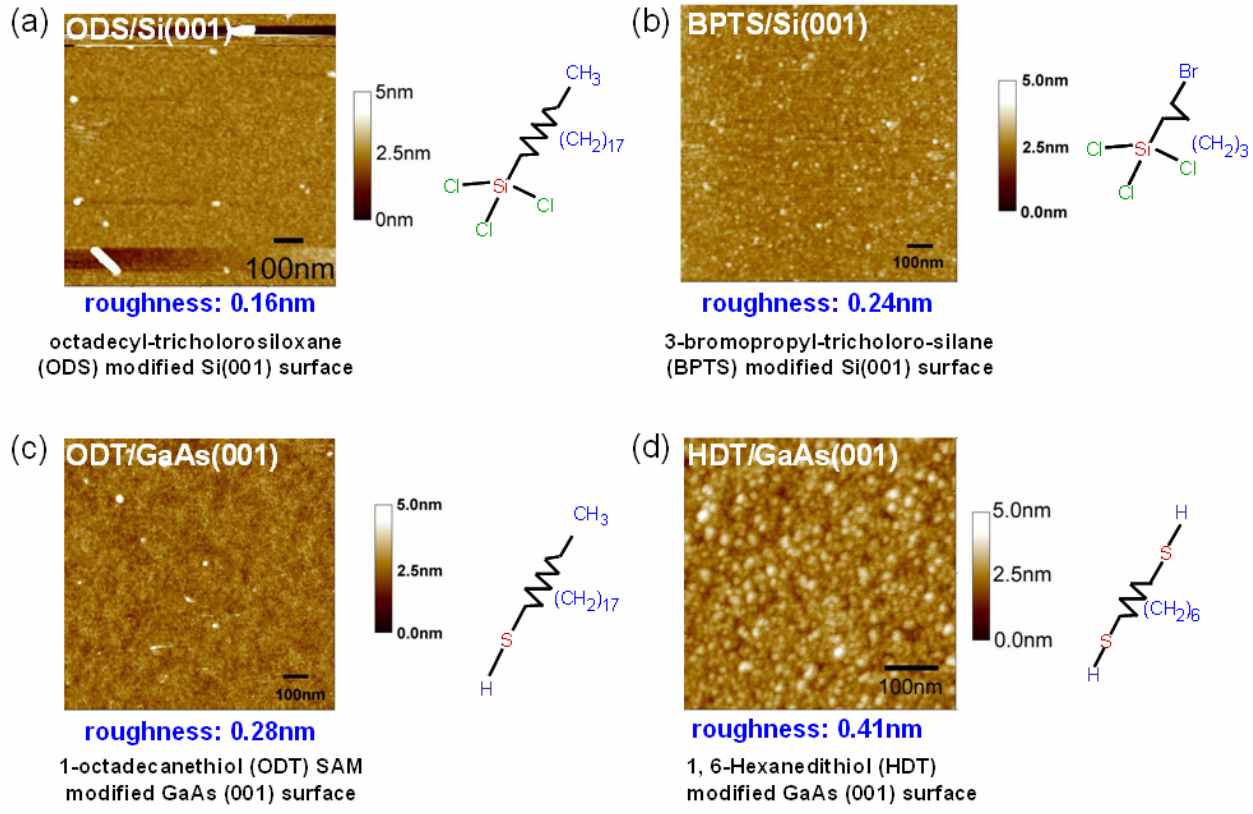

Figure 5.1 AFM image of (a) ODS modified Si(001) (b) BPTS modified Si(001) (c) ODT modified GaAs(001) (d) HDT modified GaAs(001) surfaces. The schematics to the right of the AFM images show the structure of the SAM molecules.

(b) Bio-conjugate SAMs

Following the development of protocols for the surface modification of Si, glass, and GaAs with appropriately functionalized organic SAMs as discussed in the preceding section, we moved forward to the next step in surface modification needed for subsequent attachment of proteins and cells: namely, surface modification with bio-conjugate bi-linkers that incorporate a peptide at the free-end of the organic SAM to provide molecular recognition based ligand-receptor binding for biochemical sensing. This objective is schematically depicted in Fig. 5.2 below. Denoted by red is the peptide, generically called cell adhesion molecule (CAM), which is specific for binding to the particular receptors on the protein or cell of interest.

As a vehicle for developing these ideas, our choice of specific peptides was made to leverage from efforts at USC under the NSF funded ERC on Biomimetic Microelectronics that is focused on neural prostheses. A major effort involves the ultimate objective of selective binding of neurons and glia (astrocyte) cells through the use of CAMs known to be appropriate for specifically binding these two types of cells. Given the availability of such cells under the ERC, we chose to work with designed organic self-assembling bi-linkers that at one end bind covalently to Si, glass, GaAs substrate surface and at the other end contain (a) the penta-peptide IKVAV (known to be a binding amino acid sequence within laminin, an extra cellular matrix protein) that binds to integrin, a neuron cell surface receptor, or (b) the peptide KHIFSDDSSE which binds to astrocyte cell surface receptor.

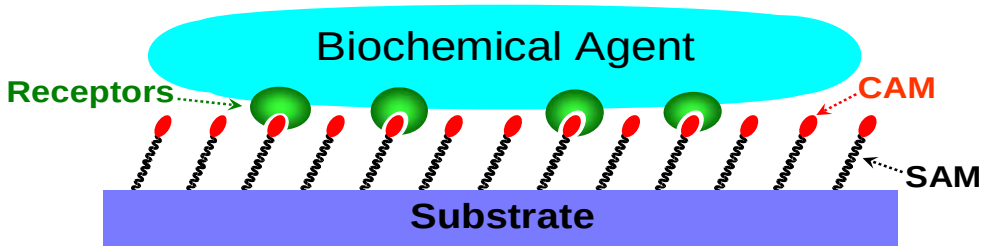

Figure 5.2 Schematic illustrating the approach to adhesion of biochemical agents (proteins, cells) onto a surface via designed peptide chains (cell adhesion molecules, CAMs).

Surface functionalization with peptides was achieved in two steps: (i) First, covalent adsorption of a self-assembled monolayer (SAM) with appropriate exposed functional groups that would allow for subsequent conjugation of the peptide of interest and (ii) Subsequent attachment of peptides onto the SAM. As illustrative examples, Fig. 5.3 shows schematics of the chemistry use for the surface modification of glass and alumina using oligopeptide CAM.

Having functionalized the surfaces as noted above, our methodology for examining the nature of the adsorbed layer at each of the two steps involves use of AFM to ascertain the degree of uniformity on the size scale of the cells themselves (~10-100 microns), and optical microscopy of dye labeled peptide-conjugated SAMs to obtain large area uniformity. An illustrative example of peptide-conjugated SAM modification of glass surface is shown in figure 5.4. The peptide coverage is seen to be fairly uniform over macroscopic (optical imaging) and nano-scale (AFM imaging) areas. Similar characterization has been performed to optimize the modification of alumina surfaces.

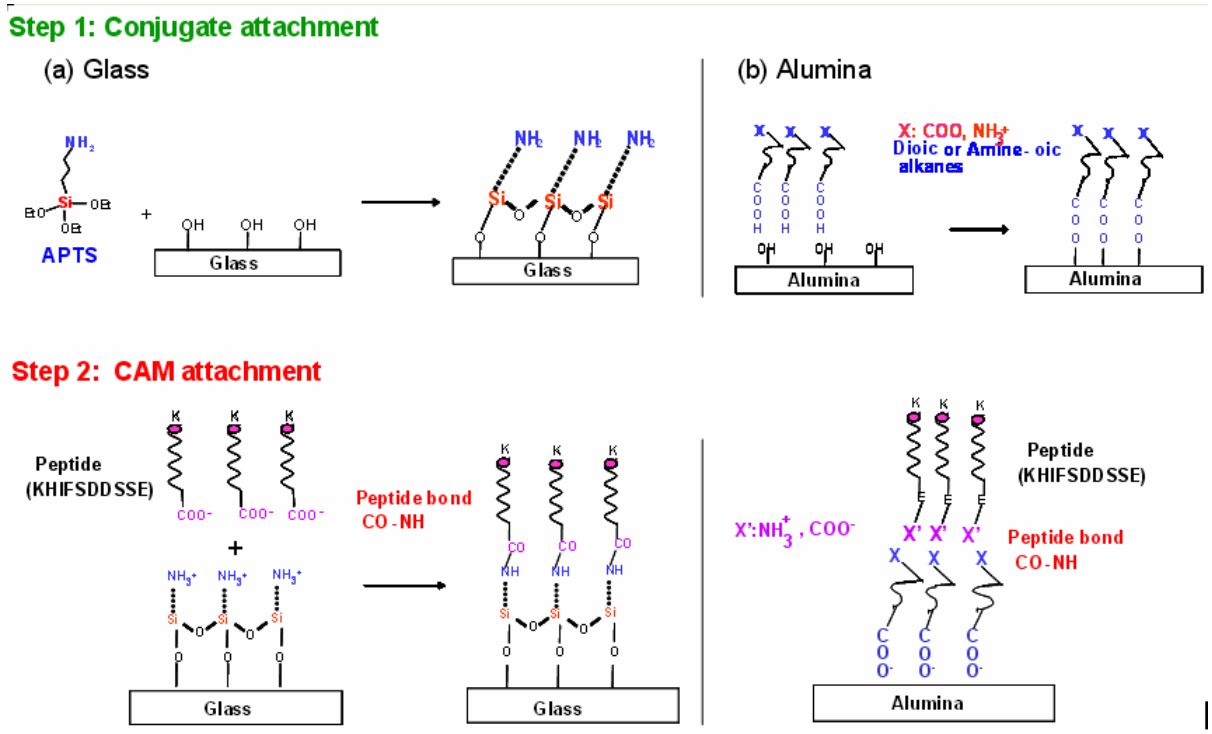

Figure 5.3: Schematic illustrating the chemistry of the peptide (KHIFSDDSSE) immobilization onto glass and alumina substrates.

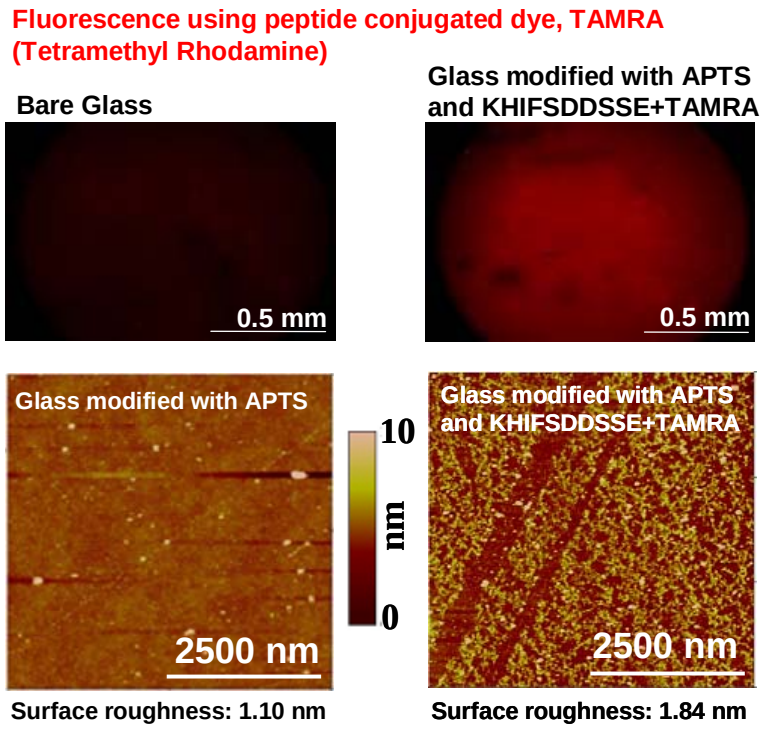

Figure 5.4. Optical fluorescence (top panel) and AFM (lower panel) images of glass surface without peptide (left) and surface reacted with peptide (right).

Such well-characterized bio-conjugate peptide (CAM) surface coatings, prepared for the first time, were used in the cell culture studies carried out in collaboration with colleagues under the NSF ERC sponsored work on neural prostheses to examine the efficacy of such CAMs for

specific (preferential) adhesion of neurons. (Results indicated that IKVAV, the neuron-specific CAM, is indeed providing selective binding of hippocampal neurons over the CAM for astrocytes and negative and positive control samples.)

II. 6. Molecular Dynamics Simulations of Alkanethiol SAMs Adsorbed on Solids (Kalia, Nakano, and Vashishta)

Publication:

S. Vemparala, B. B. Karki, R. K. Kalia, A. Nakano, and P. Vashishta, "Large-scale molecular dynamics simulations of alkanethiol self-assembled monolayers," *J. Chem. Phys.* **121**, 4323 (2004).

To complement the experimental studies of SAMs on semiconductors as noted under accomplishment 5 above, under this DURINT program, the very first molecular dynamics simulations of adsorbed organic self-assembled monolayers (SAMs) were undertaken. First, MD simulations of a thiolate SAM on Au substrate were carried out as a test vehicle for the developed interatomic potentials and scalable simulation algorithms and methodologies, while also providing a comparison with a specific class of experimental findings as a validation of the MD code for alkane thiolate, $[S(CH_2)_{12}CH_3]$. The largest system comprised a million atoms (23,040 chains). The dependence of the SAM tilt angle on the lattice constant of the solid surface was examined. The chains do not show any significant tilt when the nearest-neighbor spacing is less than 4.7 Å. With increased spacing, the tilt angle rapidly increases, which is consistent with experiments, as shown in Fig. 6.1.

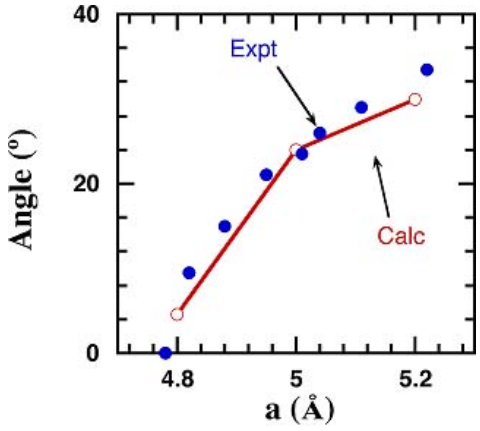

Fig. 6.1 Tilt angle of alkanethiol SAMs as a function of the lattice constant of solid surface.

Molecular Dynamics Simulation of SAMs on GaAs Surface

During this reporting period we have started MD simulations of the binding and structure of an octadecanethiol (ODT) $(S\text{-}(CH_2)_n\text{-}CH_3)$ self-assembled monolayer (SAM) on a GaAs surface. The system consists of a square lattice of sulfur atoms, bonded to GaAs substrate, which are the head group atoms of $S(CH_2)_nCH_3$ chains.

We have studied the effect of temperature on the structure of the ODT SAM with chain length n = 17 and chain-chain separation a = 7.98Å. Figure 6.2 shows that, with increasing temperature, the average tilt angle (θ) of the chains initially decreases slowly and then rapidly above 300K. At 300K the calculated tilt angle (66°) agrees fairly well with experimental tilt

angle 57±3°. The tilt direction is along the next-nearest neighbor (NNN) direction (~30º) below 300K and at temperatures above 300K it slightly increases to ~40º.

We have also observed significant effects of temperature on the existence of gauche defects. The number of gauche defects in ODT chains increases with the temperature. This can be seen from Fig. 6.3, which shows torsion angle distribution at T = 0, 150, and 300K. In this figure, gauche defects (g^- and g^+) can be seen as peaks at ± 120º. At 0K, the system is essentially gauche free.

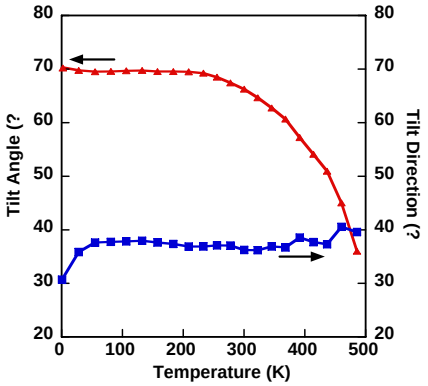

Fig. 6.2: Temperature dependence of tilt angle and tilt direction of ODT SAM on GaAs on GaAs.

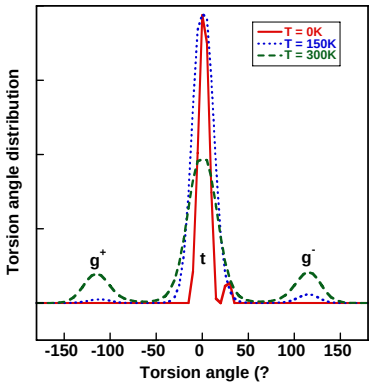

Fig.6.3: Temperature dependence of torsion angle of ODT SAM on GaAs

Structural information in X-Y plane can be probed experimentally using x-ray diffraction and surface x-ray scattering studies. Figure 6.4 shows the change in the structure factor $S(\mathbf{k})$ with the temperature. Figure 6.4a shows $S(\mathbf{k})$ with uniform tilt at temperature of 0K, whereas Fig. 6.4b shows $S(\mathbf{k})$ at 300K. The peak intensity is a function of both temperature and tilt angle of chains. At 300K, the peak intensity in $S(\mathbf{k})$ decreases from its zero-temperature value due to thermal disorder.

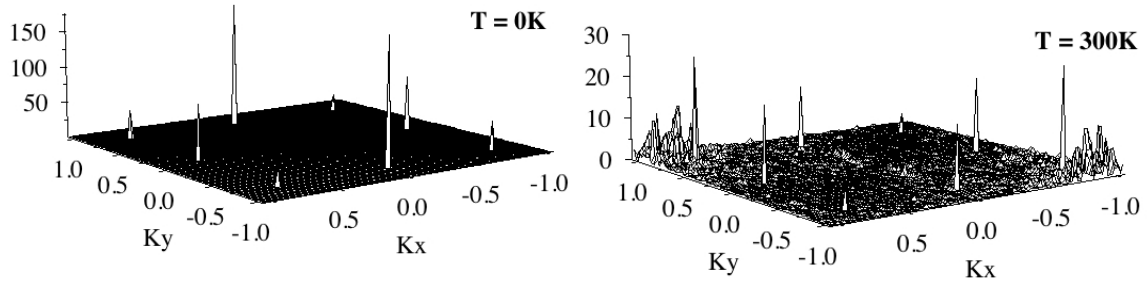

(a) (b)

Fig. 6.4: Temperature dependence of the structure factor of ODT SAM on GaAs.

The structure of the SAMs is also sensitive to the chain-chain separation a. We have studied the effect of a on the tilt angle. The separation distances, a = 3.98, 5.63, and 7.96 Å, correspond to Ga-As nearest neighbor, Ga-Ga nearest neighbor, and Ga-Ga next-nearest neighbor distances respectively. The 2d-surface plots of the tilt angle distribution are shown in Fig. 6.5. The x-y dimensions of the box are also shown. As seen in Fig. MD4, for a = 3.98 Å,

the chains are more or less standing normal to the surface, and the chains tilt ~55º when a = 5.63 Å. The case of a = 7.96 Å is also shown for comparison. It can be noted that the distribution is uniform over the system size in all the three cases.

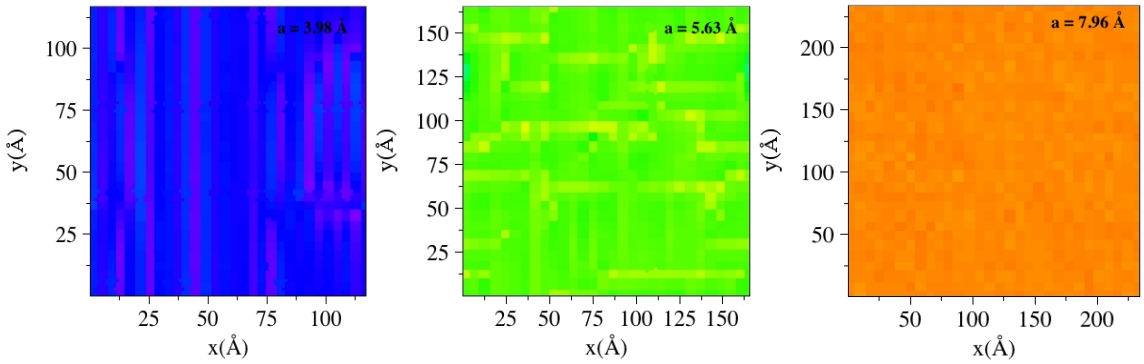

Fig. 6.5: 2D surface plots of chain-chain separation distance dependence on tilt angle in ODT SAMs on GaAs.

II. 7. Integration of biological macromolecules with colloidal nanocrystals (A. P. Alivistos et al.)

Publications:

D. Zanchet, C. M. Micheel, W. J. Parak, D. Gerion, S. C. Williams, A. P. Alivisatos, "Electrophoretic and structural studies of DNA-directed Au nanoparticle groupings." *J. Phys. Chem. B*, **106**, 11758-11763 (2002).

C. Sonnichsen, B. Reinhard, J. Liphardt, and A. P. Alivisatos, 'A molecular ruler based on plasmon coupling of single gold and silver nanopartivles", *Nat. Biotechnol.*, **23**, 741 (2005).

(a) DNA Conjugation of Nanocrystals

In the early stages of this DURINT program, a fundamental capability was developed for preparing conjugates of colloidal nanocrystals bearing a discrete and precisely controlled number of DNA originalities (single or double stranded). Under this program, the integration of oligonucleotides and antibodies with colloidal nanocrystals was a basic objective. The goal was to create a general way for bringing small numbers of nanocrystals together into well defined groupings. Thus ways to attach a specific, discrete, number, say 1 to 4 of oligonucleotides and antibodies to the nanocrystal quantum dots were developed. This was refined to demonstrate that the oligonucleotides or the antibodies can in fact be used to bring these nanocrystals together into pre-programmed arrangements. In fig.7.1 are shown illustrative examples of a CdSe/ZnS quantum dot attached through complementary DNA single strands to single, two, and three Au nanocrystals. This is an example of semiconductor-metal nanocrystal linked together through designed and controlled number of biochemical linkers. It opens the possibility of examining the nature of the response of the semiconductor quantum dot when impacted by local electric fields as may be temporally generated by exciting the plasmonic states of the surrounding metallic nanaocrystals.

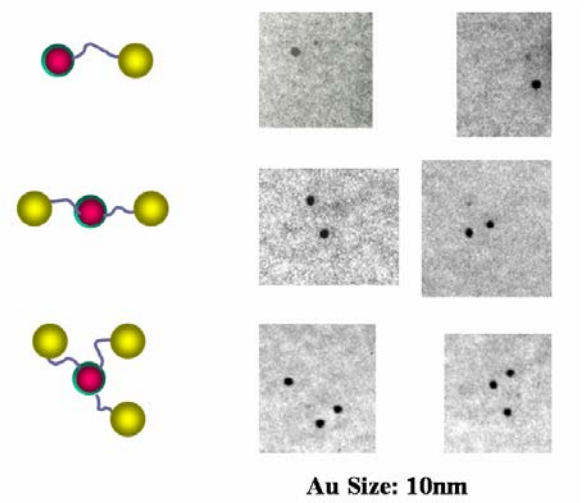

Fig 7.1. Left: Schematic of CdSe/ZnSe quantum dot attached through complementary DNA single strands to single, two, and three Au nanocrystals. Right: Corresponding TEM images of DNA conjugated CdSe/ZnSe nanocystal and Au nanocrystals.

This approach was further used for the development of two new optical detection schemes based on these new nanocrystal biomolecule assemblies. In the first, light scattering from DNA and antibody directed groupings of Au nanocrystals was examined. When the Au nanocrystals are in proximity to each other, the plasmon oscillations of one particle can couple strongly to its neighbors, resulting in a significant change in the spectrum. Thus by reading the spectrum we can determine the arrangement of the nanoparticles. The light scattering can be extremely large, providing a robust single molecule signal, and a large number of spectra can be generated by varying the number and distance of the particles. A second class of experiment involves combinations of fluorescent quantum dots with metallic nanocrystals. A combination of metallic dots located around a central colloidal quantum dot can act to enhance the local field in the vicinity of the colloidal dot, so as to greatly increase the luminescence intensity of the colloidal dot.

(b) Plasmonic Rulers:

The develop[pment of the fundamental capability for preparing conjugates of colloidal nanocrystals bearing a discrete and precisely controlled number of DNA (single or double straned), as described above, was turned into an application of these novel nanostructures as a type of spectroscopic ruler. This ruler works based on the fact that the plasmon coupling between two Au nanocrystals depends strongly upon their separation.

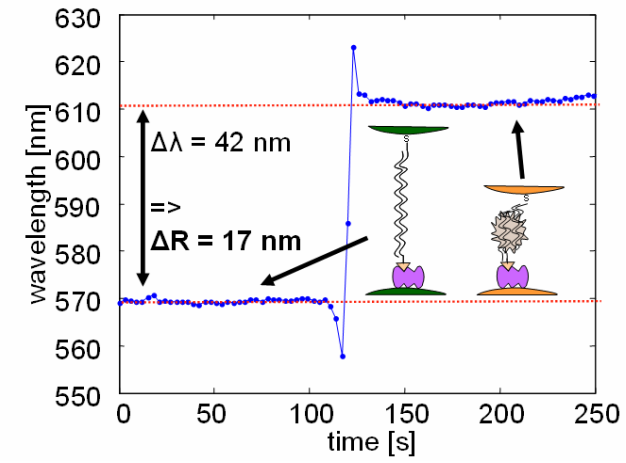

Fig..7.2 Shows the jump in the plasmon wavelength when the DNA mediated separation between a gold and a silver nanocrystal changes suddenly due to the addition of a DNA binding dendrimer.

Molecular rulers based on Förster Resonance Energy Transfer (FRET) that report conformational changes and intramolecular distances of single biomolecules have helped to understand important nanoscale processes. However, these rulers suffer from low and fluctuating signal intensities from single dyes and limited observation time due to photobleaching. The plasmon resonance in noble metal particles has been suggested as an alternative probe to overcome the limitations of organic fluorophores and the coupling of plasmons in nearby particles has been exploited to detect particle aggregation by a distinct color change in bulk experiments. We demonstrated that plasmon coupling can be used to monitor distances between single pairs of gold and silver nanoparticles. We used this effect to follow the directed assembly of gold and silver nanoparticle dimers in real time and to study the time dynamics of single DNA hybridization events. Figure 7.2 shows the jump in the plasmon wavelength when the DNA mediated separation between a gold and a silver nanocrystal changes suddenly due to the addition of a DNA binding dendrimer. These "plasmon rulers" allowed us to continuously monitor separations of up to 70 nm for more than 3000 seconds. Single molecule *in vitro* studies of biological processes, previously inaccessible with fluorescence based molecular rulers, are enabled with plasmon rulers with extended time and distance range.

II. 8. Molecular Dynamics Simulation of Adsorbed PEG Using Integrated Multi-scale Approaches Implemented on Parallel Computing Platforms (Kalia, Nakano, and Vashishta)

Publication:
S. Vemparala, R. K. Kalia, A. Nakano, and P. Vashishta, "Electric field induced switching of poly (ethylene glycol) (PEG) terminated self-assembled monolayers: a parallel molecular dynamics simulation," *J. Chem. Phys.* **121**, 5427 (2004).

As noted under the objectives, a central part of the integration of epitaxical and colloidal nanostructures to realize hybrid device structures suited for biological applications involves functionalizing surfaces with organic and/or peptide SAMs. Atomic force microscope images of the morphology of organic SAMs functionalizing Si and GaAs, and of SAMs further conjugated with peptides of relevance to cell adhesion, obtained under this DURINT program are illustrated under accomplishment 5. To move towards developing the capability of simulating such systems, under this program, MD simulations of poly ethylene glycol (PEG) modified alkanethiol SAM on simulated Au surfaces were developed. Poly ethylene glycol (PEG) is used very often as a stabilizing surface coating material in biological environments due to low toxicity and hydrophilic nature combined with its inertness towards protein adsorption. The surface structure, helical nature of PEG, crucial to its protein resistance properties is very sensitive to external parameters such as temperature, electric field and type of substrate. Experiments at MIT [J. Lahann, et al., *Science* **299**, 371 (2003)] had shown a reversible effect of electric field on self-assembled monolayer (SAM) structure, demonstrating a viable field-induced surface switch. Thus, molecular dynamics (MD) simulations to understand the effect of electric field on the helical nature and the structure of the polyethylene glycol (PEG) SAMs were undertaken.

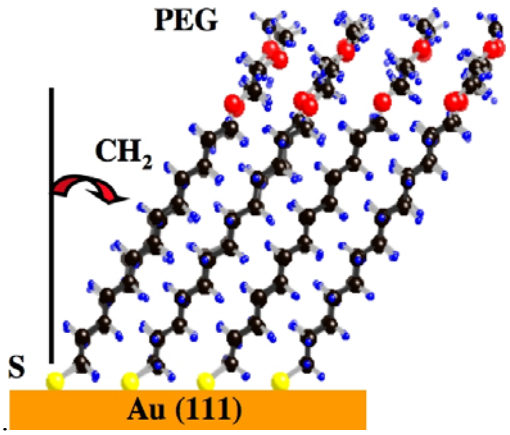

Fig. 8.1 Schematic of PEG (S-$(CH_2)_n$-(O-CH_2-$CH_2)_m$-O-CH_3), where typically n = 13 and m = 3.

First, the structure of PEG-SAMs in the absence of electric field was studied (see Fig.8.1). SAMs usually adopt a (√3x√3)R30° triangular lattice in the x-y plane and tilt ~30° from the z (normal) axis. Heating and cooling cycles show hysteresis in tilt angle. The loss of tilt angle (hence order) at higher temperatures is reminiscent of 2D melting. Tilt angle of 29º at 300K agrees well with experimental value of 30º± 2º. Unique helical nature implicated in excellent hydrophilic nature of PEG has a signature of C-C gauche bond peak in the radial distribution function (RDF). As more space is available, ability to form helical structure increases, and the O-O distance acquires a peak ~3Å.

In the MD simulations of electric-field switching (see Fig.8.2), the reversible effect of the positive electric field manifests itself as regaining of hydrophobic surface (hydrogen) after the removal of electric field. This can also be seen in the regaining of trans peak (~4Å) in the radial distribution function with removal of electric field. 90% of the tilt angles in alkane chains are also regained. Negative potential affects the tilt structure more adversely than positive potential.

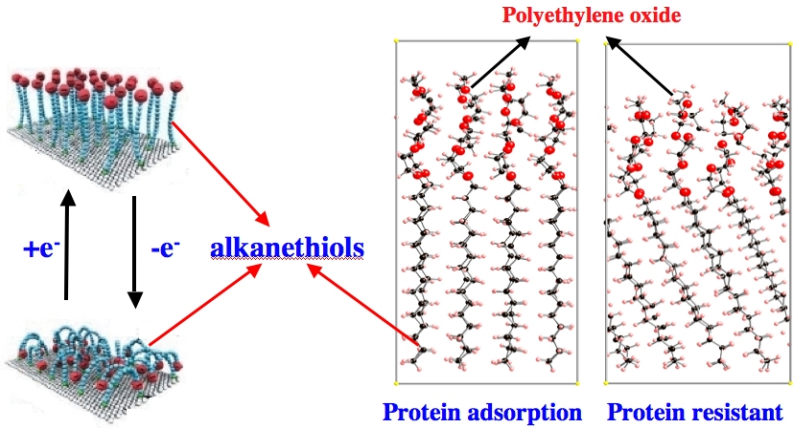

Fig.8.2 (Left) Hydrophilic-hydrophobic switching by applied electric filed switching. (Right) Protein adsorption-resistant switching of PEG-SAM by applied electric field.

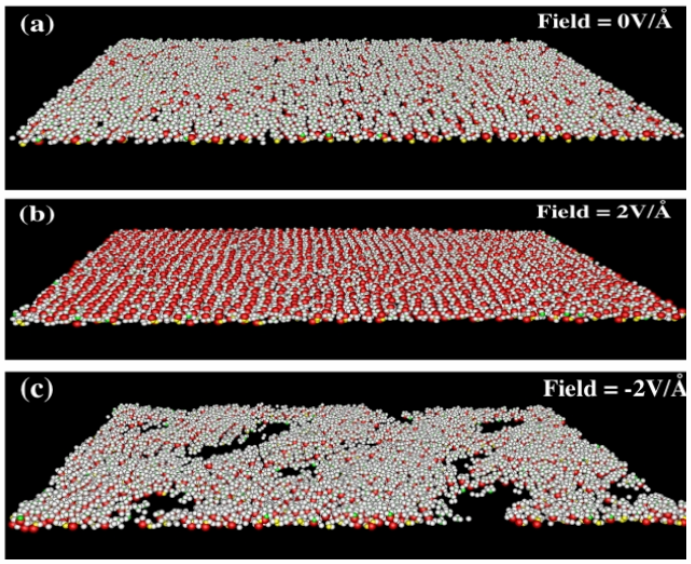

Figure 8.3. The atomic configuration color coded by charges: oxygen (red), hydrogen (white), methyl terminal carbon (yellow) and carbon in PEG (green) in top 6Å layer of the SAMs: (a) $E_z = 0$, (b)$E_z = +2$V/Å, and (c) $E_z = -2$ V/Å.

Results of the MD simulations carried out to study the effects of electric field on the structure of poly-(ethylene glycol) (PEG) terminated alkanethiol SAM are shown in fig.8.3. An applied electric field triggers a conformational transition from all-trans to a mostly gauche conformation. The polarity of the electric field has a significant effect on the surface structure of PEG, in particular on the hydrophilicity of the surface. The electric field applied anti-parallel to the surface normal causes a reversible transition to an ordered state, in which the oxygen atoms are exposed. On the other hand, an electric field applied in a direction parallel to the surface normal introduces considerable disorder in the system and the oxygen atoms are buried inside. The parallel field affects the overall tilt structure of SAMs more adversely than the anti-parallel field. Such conformational changes could cause reversible switching of hydrophilicity in SAMs, as was demonstrated in a recent experiment.

II. 9. Energy Transfer from Nanocrystal Quantum Dot to Near-Surface Quantum Channel: Time-Resolved Photoluminescence (Lu, Madhukar)

Publication:

S. Lu and A. Madhukar, "Nonradiative Resonant Excitation Transfer from Nanocrystal Quantum Dots to Adjacent Quantum Channels", Nano Lett., (2007).

In order to examine the dynamics of energy transfer in the nanocrystal/substrate hybrid structure revealed by the integrated PL discussed under item (1) in the preceding, we established a time-resolved photoluminescence (TRPL) setup. In our TRPL setup, a fs cavity-dumped mode-locked Ti:S laser is used for excitation and an infrared enhanced micro-channel plate PMT is used for time-correlated single photo counting detection. In fig.9.1 is shown the electronics limited instrumentation response function (IRF) of the current TRPL setup. The full width half maximum of the IRF is 27ns. After deconvolution a time resolution of ~20ps can be achieved.

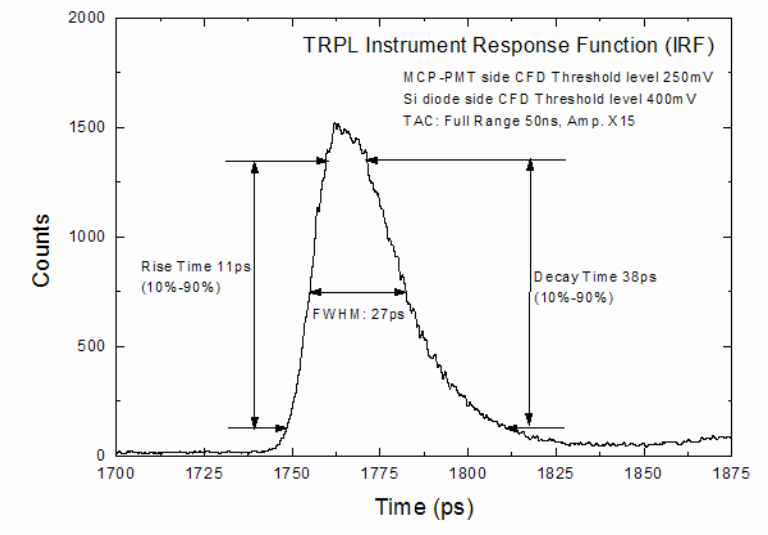

Fig 9.1. Instrument response function of the current TRPL setup.

(a) Foster Resonant Transfer between Nanocrystal Quantum Dot and Near Surface Quantum Well (NSQW)

As the first application of the TRPL technique, we examined Förster Resonant Energy Transfer (FRET) between NCQDs and near surface quantum well (NSQW). The system investigated is PbS nanocrystals (emission 950nm) deposited on a GaAs substrate with InGaAs near surface quantum well (NSQW) (emission 1010nm) buried ~5nm below (Fig.9.2). Here PbS nanocrystals are chosen for its emission wavelength matching to the absorption of our InGaAs based QWs to allow FRET to happen. First indication of nonradiative resonant energy transfer came from experiment run in February of 2005 and reported in the Annual Progress Report for 7/1/2004-6/30/2005. This data, shown here in fig.9.3, is the fluorescence decay of PbS NCQDs on a GaAs substrate with (red) and without buried InGaAs NSQW. The excitation was kept below the GaAs bandgap so that only NSQW and NCQDs are excited. In the presence of the buried near-surface InGaAs quantum well the PbS nanocrystal quantum dots show a decreased fluorescence lifetime compared to PbS on GaAs without NSQW, indicating a FRET type transfer from NCQD into the NSQW.

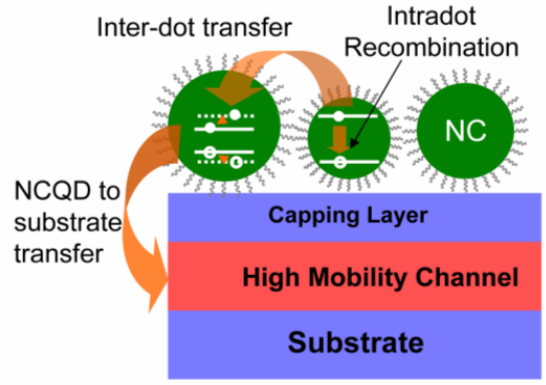

Fig. 9.2**.** Schematic of ligand-capped NCQDs deposited on near surface epitaxial quantum nanostructure. Orange arrows indicate the competing intradot recombination, interdot nonradiative energy transfer, and NCQD-to-substrate nonradiative energy transfer processes

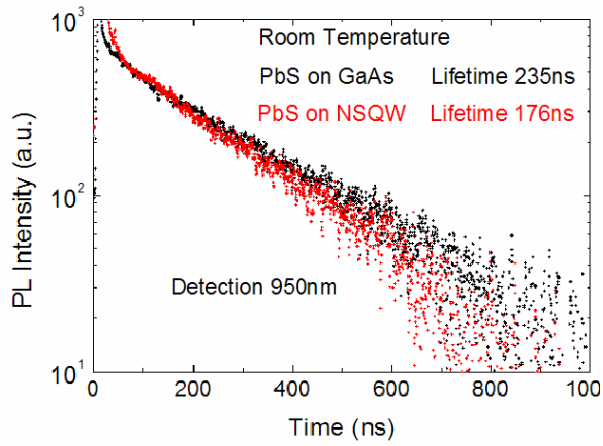

Fig 9.3. Room temperature fluorescence lifetime of PbS NCQD (emission 950nm) on a GaAs substrate with (red) /without(black) a buried InGaAs NSQW (emission 1010nm). Excited at 900nm below GaAs bandgap.

Given the significance of the ability to control composite nanostructures to induce nonradiative resonant energy transfer, effort was spent in improving the instrumentation and the preparation of the appropriate composite structures to improve the signal to noise ratio over that of the first experiments shown in Fig.9.3 above.

With improved signal to noise ratio, systematic studies were carried out for the PbS NCQDs – GaAs/InGaAs/GaAs system noted above. This included reference studies for PbS NCQDs adsorbed on glass substrates to establish the inter-NCQD FRET rate (Fig.9.2) as this process is responsible for the transfer of absorbed energy in the smaller NCQDs (with higher bandgaps) to the larger NCQDs (with smaller band gaps but resonantly matching, within thermal uncertainity, excited states). The PL intensity decay of the typical smaller and larger NCQDs in the distribution are shown in Fig.9.4(a) for their emission at 900nm and 965nm, respectively. Note that the InGaAs quantum well to which energy is aimed to be resonantly transferred in the composite structure is designed to absorb (i.e. accept emission) at ~965nm. To confirm that the observed difference in the decay rates of the smaller and larger NCQDs in the distribution of sizes is representative of the interdot transfer, the decay rates were measured as a function of temperature, as shown in Fig.9.4(b). The temperature independence of the decay time constant for the smaller dots, while the temperature variation seen for the larger dots, clearly demonstrates that rapid resonant transfer from the smaller to the larger dots is occurring. The behavior of the PbS NCQDs on GaAs surfaces with (red) and without (blue) the near-surface InGaAs quantum well is shown in Fig. 9.5. The enhanced decay in the presence of the quantum well is indicative of nonradiative resonant energy transfer (NRET) from the NCQDs to the quantum well. Analysis of the decay rates, provided in detail in the published paper in Nano Letters noted at the beginning of this subsection, showed that, for the PbS quantum dots used here having 30% quantum yield, the nonradiative resonant transfer rate to the NSQW channel is ~30%. For near unity quantum yield dots, as can now be produced, this transfer rate would be ~60%. An important information to note here is that these values are for an estimated separation between the NCQDs and the center of the quantum well of ~8.2nm. If this separation is reduced through proper design to ~6nm, it will gain a factor of four in the resonant transfer rate and push the transfer efficiency from 60% to ~84%.

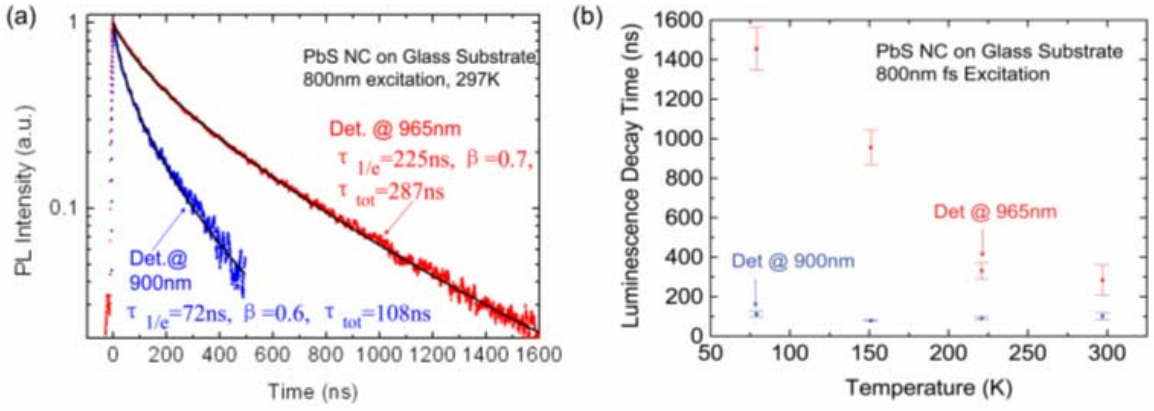

Fig. 9.4 (a) Illustrative example of time-resolved PL of PbS NCs on glass substrate at 297K, detected at the PL peak wavelength of 965nm (red) and at 900nm (blue). The TRPL spectra are fitted with stretched exponential functions (black solid curves), which give mean total luminescence decay time (τ_{tot}) of 287ns and 108ns for emission at 965nm and 900nm, respectively, from the most probable and smaller size NCs. (b) Measured temperature dependence of the total luminescence decay time (τ_{tot}) detected at 965nm (red) and 900nm (blue). Note the decay time at 900nm is limited to ~ 100ns and independent of temperature, indicating rapid inter-dot energy transfer.

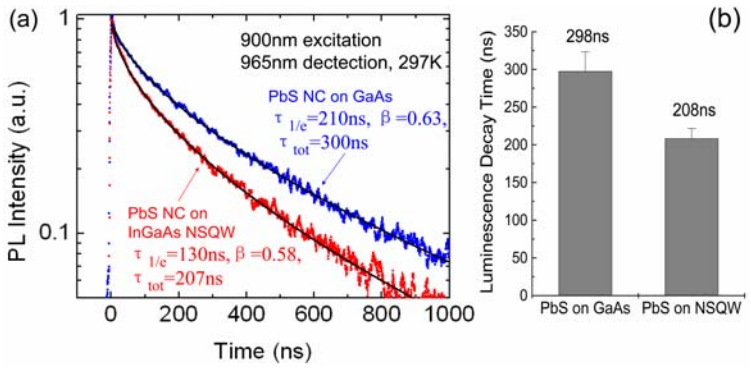

Fig. 9.5 (a) Time resolved PL of PbS NCs on passviated GaAs (blue) and on passivated NSQW (Red). Excited at 900nm (below GaAs bandgap) and detected at 965nm (PbS PL peak). The decay of the TRPL curves are fitted using stretched exponential function. (b) Mean luminescence decay time (τ_{tot}) of PbS NCs (detected at 965nm) on GaAs and on NSQW. Error bar shows the standard deviation of the measured decay times from five different spots on each sample.

(b) NRET Based Photovoltaic Solar Energy Conversion

The above findings indicate that NRET in suitably designed composite NCQD-epitaxial nanostructures offers a new class of structures for potentially efficient conversion of solar energy to power. Such studies are being pursued under AFOSR sponsorship following the completion of this DURINT program. An illustrative schematic of the type of solar cell architectures being pursued is shown in Fig.9.6.

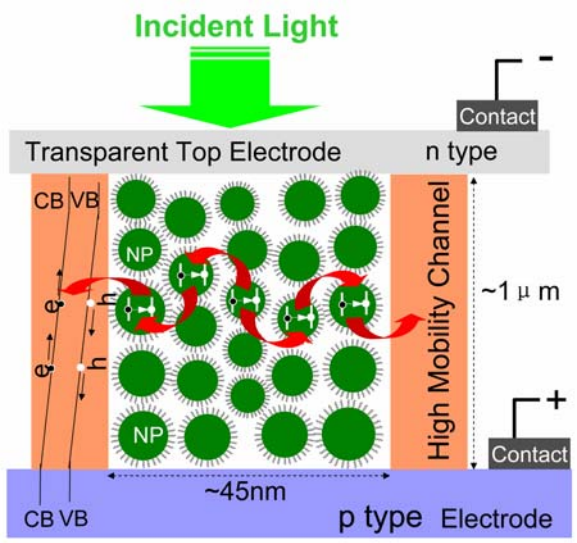

Fig. 9.6 Schematic showing an architecture comprising nanocrystal absorbers embedded in a vertical array of high mobility channels that allow nonradiative transfer of excitons from the adjacent NCQDs and simultaneously provide high mobility transport.

II. 10. Combined Quantum mechanical-Classical Simulations of Charge transport in Excited State of an Organic Molecule (Kalia, Nakano, and Vashishta)

To study electron transport in hybrid bio/colloidal/epitaxial structures, we have developed a quantum electron transport simulation method. This method simulates the time evolution of an excess electron wave packet by numerically integrating the time-dependent Schrödinger equation. We have tested the simulation method on excess electron transport in a hexadiene (C_6H_{10}) molecule. The electron-molecule interaction is described by a psuedopotential developed by Prof. Vince McKoy (Caltech) based on self-consistent field calculations using the GAMESS software. The pseudopotential includes the effects of polarization and exchange. The left and right panels of figures 10.1 show, respectively: (1) a projection of a 2,4-hexadiene molecule on the x-y plane, where red and blue circles represent C and H atoms; and (2) the electron-hexadiene pseudopotential as a function of x and y coordinates on the z = 0 plane.

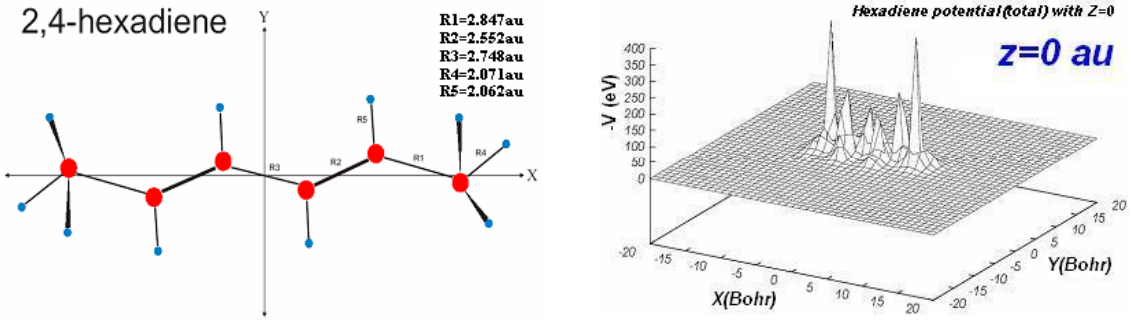

Figure 10.1**.** (Left) Projection of a 2,4-hexadiene molecule on the x-y plane, where red and blue circles represent carbon and hydrogen atoms, respectively. (Right) The electron-hexadiene pseudopotential as a function of x and y coordinates on the z = 0 plane.

We have simulated the dynamics of an excess electron wave packet with an incident velocity of 105 m/s. The findings are shown in Fig.10.2. The top-left figure is a schematic of the

simulation. The other figures show a time sequence of the probability density of the excess electron as a function of the x and y coordinates at the z = 0 plane. The simulation reveals the localization of the excess electron at the carbon double bonds.

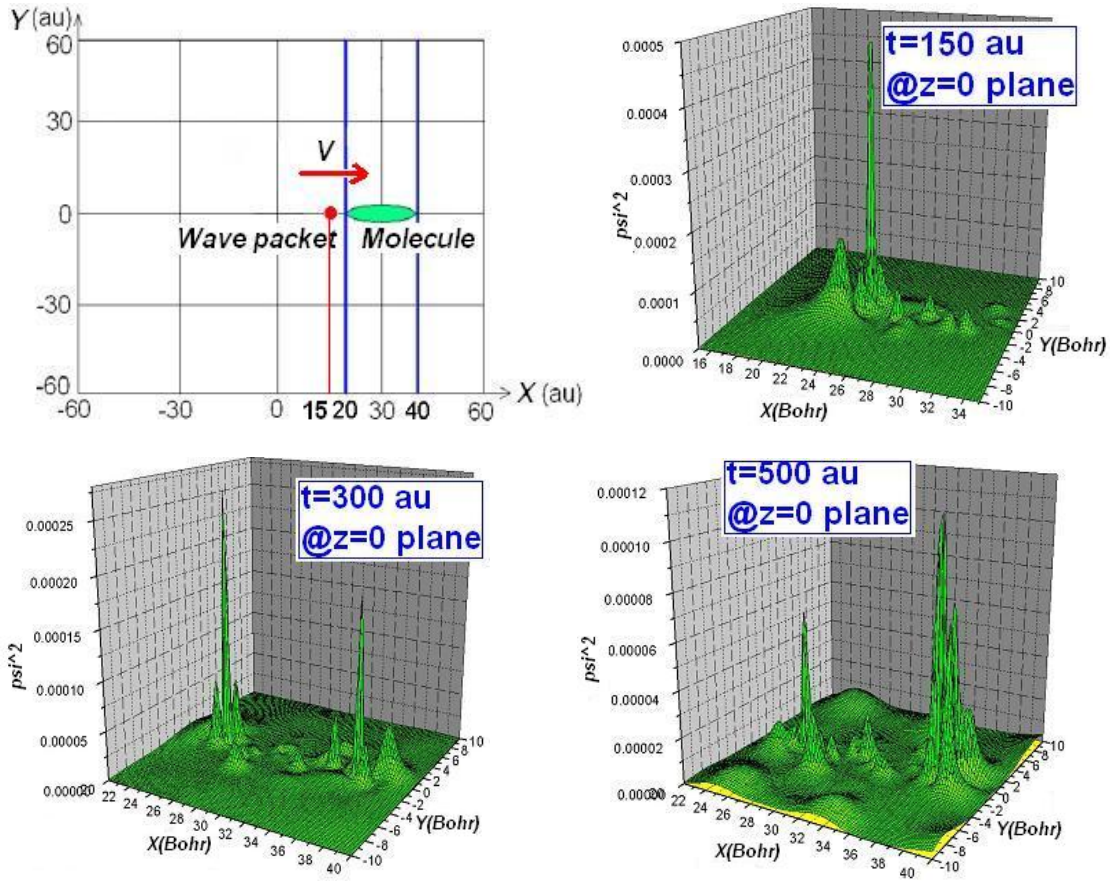

Fig.10.2 Shows the findings of the simulation of the dynamics of an excess charge across the 2,4-hexadiene molecule shown in Fig.10.1.

II. 11. Semiconductor-Metal Nanocomposites: Schottky NanoPhotodiodes (Madhukar)

While individual nanocrystals made of semiconducting, metallic, or ceramich materials had become and remain common-place, and even their combinations are linked together through appropriate molecular bilinkers, epitaxically-integrated semiconductor-metal nanocrystals were hardly examined. Yet, arguably the earliest and one of the more pervasive semiconductor device is the semiconductor-metal (Schottky) diode. We thus set out to demonstrate the first Nano-Schottky diode by undertaking epitaxy of metal on semiconductor nanocrystal rods in solution based colloidal chemistry. The particular challenge faced and reasonably overcome was controlling such metal epitaxy only on one side of the semiconductor rod.

(a) Synthesis and TEM (Lu, Hughes, Alivisatos, Madhukar)

The CdSe/Au integrated nanocrystalline composites were synthesized through a two-step procedure. First, CdSe nanorods were formed by the reaction of Cd and Se precursors in a mixture of trioctylphosphine oxide and an alkylphosphonic acid. Because the (001) and (00$\underline{1}$)

facets at the two ends of the rods have a higher chemical potential than the {011} facets at the sides of the rods, the ends tend to adsorb the alkylphosphonic acid, while the sides preferably adsorb the trioctylphosphine oxide. Second, the CdSe rods suspension is treated with a mixture of gold chloride, didodecyldimethylammonium bromide, and hexadecylamine to stabilize the nanocrystals and to rreduce the gold chloride to elemental gold. Because the two ends ((001) vs. (00$\underline{1}$) facets) of the CdSe rods differ crystallographically (and hence chemically), careful control of growth conditions allows growth of Au particles preferentially on one end of each rod. Figure 11.1 shows high-resolution transmission electron microcope images of CdSe/Au nanocrystalline semiconductor/metal heterojunctions. The dark end of the rod corresponds to the Au tip, which has higher electron density than the CdSe end. The particle size (< 2 nm to > 100 nm), aspect ratio (1:1 to > 1:30) or shape (rod, tetrapod) can be varied over a wide range by controlling growth conditions.

Fig. 11.1 HRTEM image of Au/CdSe junction. The majority of CdSe rod structure integrity is maintained as evident from the observed CdSe lattice image.

(b) Photovoltaic Response of CdSe-Au Schottky Nanocomposites (Lu and Madhukar)

The photovoltaic effect of the CdSe/Au FAN is also independently checked using atomic force microscopy (AFM) based surface potential probing (SPP) as schematically shown in figure 11. To prepare the sample for this measurement, a drop of CdSe/Au FAN solution in toluene was put onto a freshly cleaved surface of highly ordered pyrolytic graphite (HOPG) and placed in an electrical field of ~1x10^{4}V/cm perpendicular to the HOPG surface. Since the CdSe/Au FANs have built-in electrical dipole, as the FAN solution slowly dries (over ~ 1 hour), the HOPG surface gets coated with a layer of FANs that statistically acquire a preferred orientation along the electrical field perpendicular to the surface.

The sample was then installed on a Digital Instrument Multimode AFM and an Iridium-coated conducting AFM tip was used to measure the surface potential ($V_{surface}$) of CdSe/Au FAN coated HOPG substrate under light excitation as briefly described below (refer to figure 11.4). The AFM tip was lifted a certain height (~60nm) above the surface of the sample. A voltage $V(t)=V_{DC}+V_{AC}\cdot\sin(\omega t)$ was applied on the AFM tip (where ω is the resonant frequency of the tip) to create an oscillating electrical force between the tip and the surface. The surface potential ($V_{surface}$) was then measured by adjusting V_{DC} to be equal to $V_{surface}$ via a feedback loop so that the force between the tip and surface at frequency ω was zeroed (hence the oscillation of the tip is minimized).

In our measurements, the FAN coated HOPG sample was excited by a 532nm laser chopped at 10Hz. The measured surface potential is shown in figure 12. The difference in the surface potential as the light excitation is turned on and off is around 15mV. This difference can most likely be attributed to the photovoltaic effect of the CdSe/Au FANs on the HOPG surface, since no measurable surface potential change as a function of light excitation was observed on either bare HOPG or HOPG surface deposited with CdSe rods.

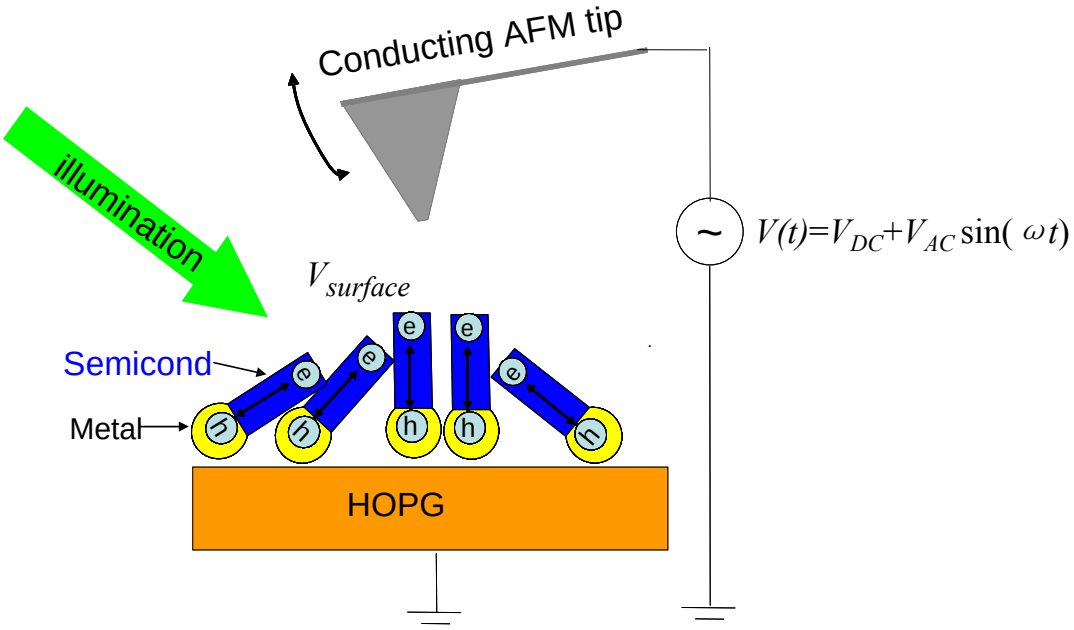

Figure 11.4. Schematic showing the experimental setup used to probe the photovoltaic effect of FANs using atomic force microscopy based surface potential probing (SPP). See text for details of the measurement.

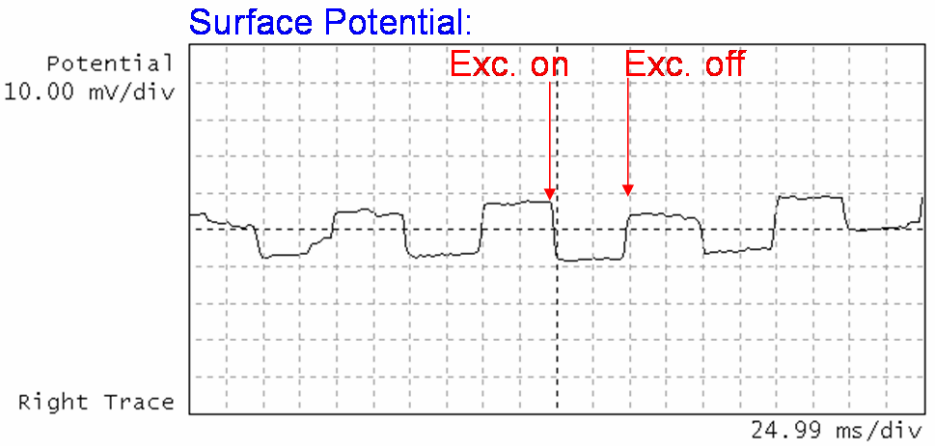

Figure 11.5. Measured surface potential change of FAN coated HOPG substrate under illumination by 532nm laser chopped at 10Hz. A surface potential difference of ~15mV was observed when illumination is turned on and off. This difference may be attributed to the photovoltaic effect of the FAN.

II. 12. Nanoscale Near-Field Optical Imaging (Lu, Madhukar)

Simultaneous AFM & NSOM based Imaging of Labeled Cells:

In this DURINT program substantial effort was invested on *nanoscale* spatially-resolved imaging of biological systems. Such efforts are motivated by the need to acquire fundamental understanding of the target biological systems for the appropriate design of chip-based bio-sensors. Such efforts not only benefited the realization of other DURINT objectives, the unique instrumentation capability established along the way is enabling grand-breaking research and is showing its impact even beyond the time period of DURINT. In a previous section is discussed the imaging of proteins using transmission electron microscopy and atomic force microscopy performed in liquid environment. This section documents briefly our DURINT supported work on combined AFM and near-field optical microscopy of cells.

As depicted in our scheme of chip based bio-sensing using quantum nanostructures buried near substrate surface, the membrane receptors of relevant cells are in contact with a substrate, hence are playing a critical role. To acquire the density and distribution of surface receptors (information that previously did not exist in the literature due to the lack of suitable characterization means), a surface sensitive cell imaging technique with nanometer scale spatial resolution is required. For this purpose, we have developed a unique imaging setup, utilizing normal force AFM based near field optical microscopy (NSOM), for simultaneous 3D morphological and surface-sensitive fluorescent optical imaging of cells.

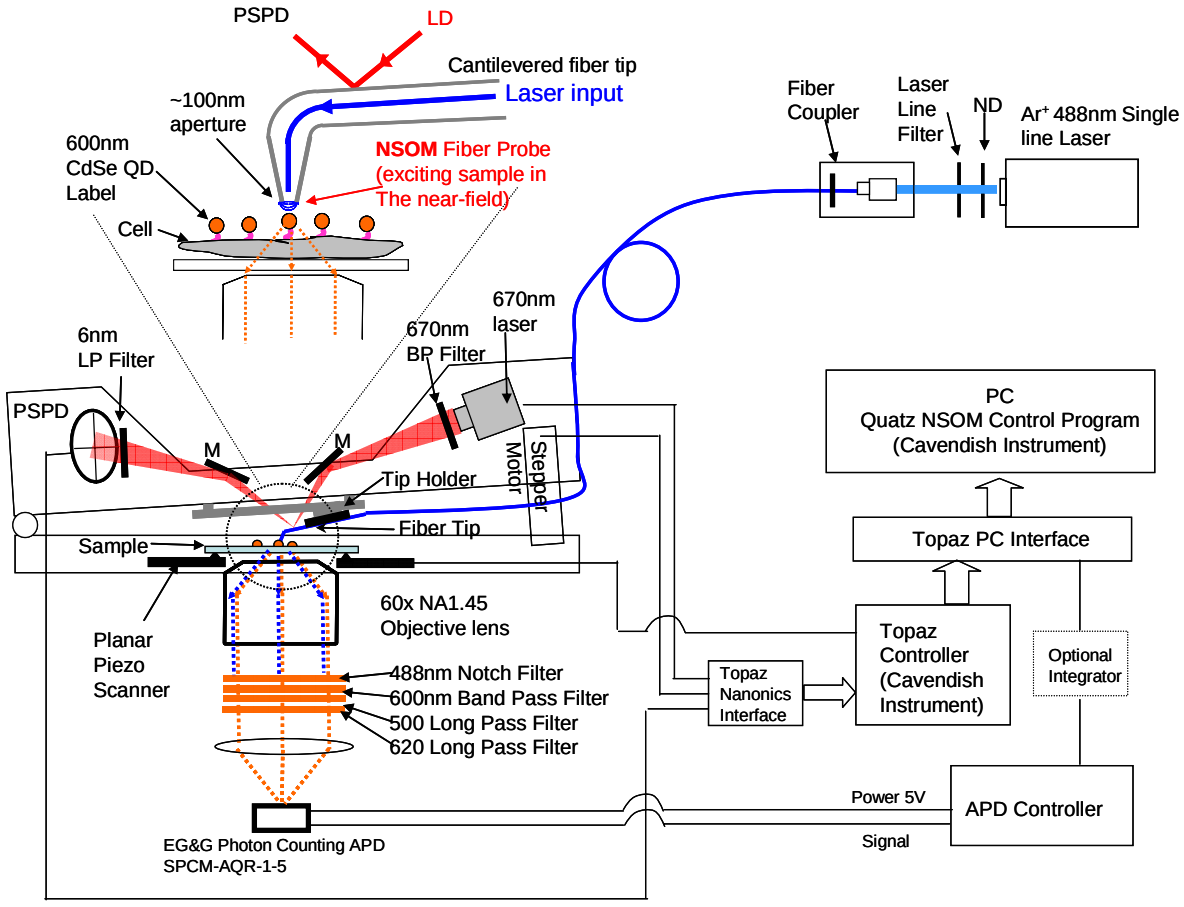

Figure 12.1 Schematics of our combined AFM/NSOM system for simultaneous 3D morphological and surface-sensitive fluorescent imaging of cells

The schematic of the combined NSOM/AFM system is shown in figure 12.1. It works very similar to a normal force tapping mode AFM, except that the conventional AFM tip is now replaced by a cantilevered optical fiber with a sub-wavelength aperture ~50-100nm in diameter at one end. Such a tip acts both as an AFM tip for morphological imaging and as an optical fiber to transmit light for optical imaging. The excitation light injected into the tip diffracting through the sub-wavelength aperture creates a near field at the end of tip which excites almost exclusively only fluorophores on the surface of a cell. This gives NSOM technique its exquisite surface sensitivity. Further, utilizing near-field excitation, the resolution of NSOM is decided by the diameter of the aperture. This breaks the usual diffraction limit of optical microscopy and allows the distribution of cell surface receptors on the nanoscale to be revealed.

As collaboration opportunity arose within USC, the AFM/NSOM system was used to study breast cancer cells and the distribution of surface receptor Her2/neu, a known oncoprotein connected to the occurrence and prognosis of different types of breast cancers. As an illustrative example, in figure 12.2, we show a high resolution simultaneous AFM and fluorescent NSOM image of a partial area of a SKBR3 breast cancer cell (panel (a) and (b)) and a MDA breast cancer cell (panel (c) and (d). For fluorescent NSOM imaging, the Her2/neu receptors on the cell

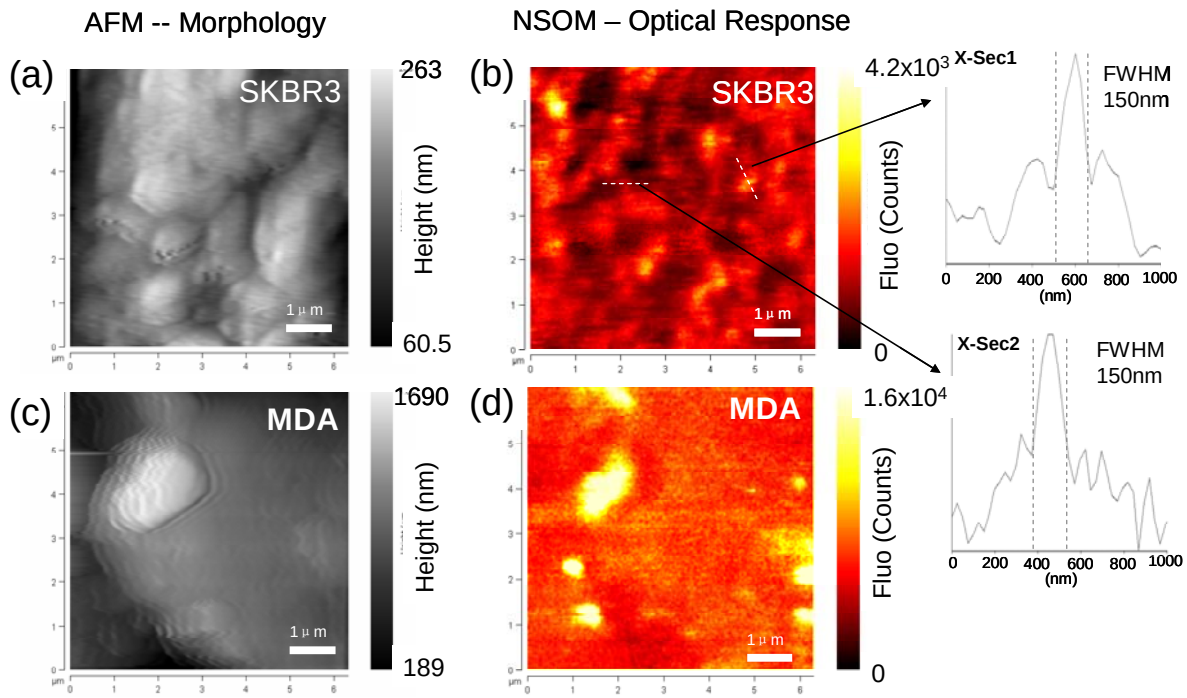

Figure 12.2 Simultaneously obtained AFM and fluorescent NSOM images of QD (CdSe/ZnS 605nm) labeled SKBR3 cells (panel a, b) and MDA cells (panel c, d). Image obtained with tip of 100nm diameter aperture. Insets (XSec1) and (XSec2) show two cross-sections on the NSOM image (panel b) to illustrate the smallest features on the image. The resolution of the image as demonstrated by the FWHM of such feature is <150nm.

membrane were labeled using quantum dots (CdSe/ZnS QD, 600nm emission) conjugated with anti-Her2/neu antibodies. The resolution of the NSOM images is ~150nm (see figure 12.2 inset Xsec1 and Xsec2) beyond the diffraction limit. The fluorescent NSOM images (figure 12.2c and

12.2d) revealed that the Her2/Neu receptors are not distributed evenly on the surface of these two types of breast cancer cells but instead are localized in clusters ~500nm in diameter. The number of such clusters of Her/neu on MDA is much smaller than on SKBR3 cell. The clustering of the Her2/neu receptors, as observed in these beast cancer cells, may have important role in the pathogenesis of beast cancer and may provide a strategy for designing a chip-based biosensor to distinguish cancer cells vs. normal cells.

Following the establishment of the AFM-based NSOM to enable simultaneous morphological and near-field optical imaging on nanoscale as demonstrated above, attention was focused on near-field optical studies of the hybrid NCQDs adsorbed on a solid substrate structures such as discussed earlier under item (1) of this section. In Figure 12.3(a) is shown an early NSOM image of single CdSe/ZnS core-shell quantum dots (~600nm emission) sparsely dispersed on a glass substrate. The image was acquired using an NSOM tip with a 500nm diameter aperture and a 5mW 532nm Nd:YAG for excitation. Each bright yellow spot on the image corresponds to the fluorescence from a single QD.

Beyond imaging, efforts were spent to add the capability for spectrally-resolved and temporally-multiplexed detection for advanced optical studies of biomolecular processes. In Figure 12.3(b) is shown an illustrative example of a PL spectrum from a sample comprising QDs on a glass substrate (sample similar to the imaged in figure 12.3(a)) measured using the NSOM system. The PL signal was collected from a local area on the sample using a 500nm diameter aperture NSOM tip. The observed full width at half maximum (FWHM) of the PL peak is ~5nm (limited by the resolution of the 1/8 meter spectrometer employed), far narrower than the FWHM of the photoluminescence peak of the CdSe/ZnS QD ensemble in solution (~30nm). The PL signal thus most likely arises from a single CdSe/ZnS NCQD. These capabilities, established during this DURINT program, are being employed for a variety of follow-through and new studies.

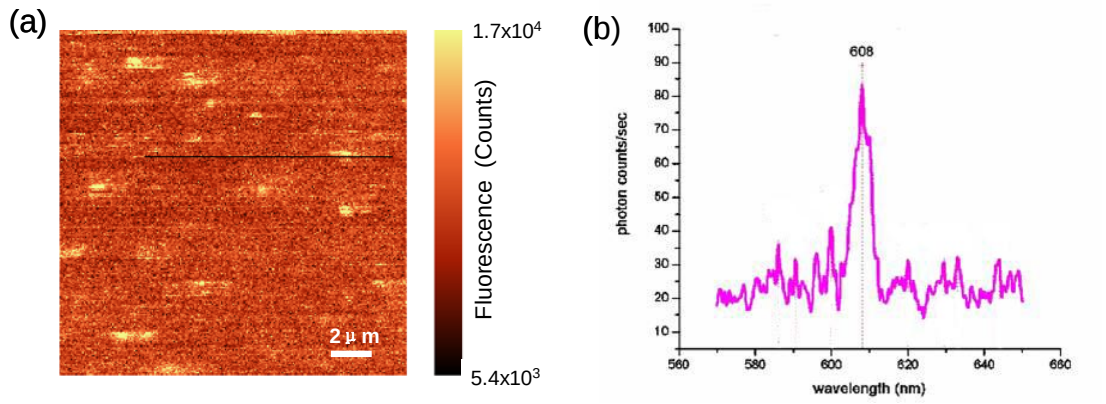

Figure 12.3 (a) An NSOM image of single 600nm CdSe/ZnS QDs sparsely dispersed on a glass substrate. (b) A photoluminescence spectrum of a CdSe/ZnS QD measured using NSOM.

Other Findings:

II. A. Protein Adsorption on Solid Substrates

A component of our DURINT program envisions surface modification via peptides/proteins to create templates with the objective of directed-assembly of nanocrystal quantum dots through appropriate chemical functionalization. Consequently, our efforts focused upon careful and systematic studies of protein adsorption from solution onto solid substrate. Two types of substrates are used: (a) carbon-coated TEM grids and (b) solid surfaces such as mica, Si, and GaAs. For the former, TEM imaging is utilized and for the latter AFM imaging in solution is employed to resolve the structure of adsorbed proteins and the protein arrays. Below we document some illustrative images from the TEM and AFM studies, respectively.

- **Study of Self-Assembled 2D Chaperonin on TEM Grid**

For directed-assembly of nanocrystal quantum dots on solid substrate, this PI recognized that an excellent candidate to serve as the protein template is the β-subunits of TF55 from Sulfolobus shibatae, that belongs to the class of proteins called Chaperonins.

Colleagues at NASA's AMES Laboratory (Astrobiology Division) had been examining this protein that is stable under extreme conditions (high temperatures) and we suggested its potential use as a template for building nanoparticles. This led to collaborative efforts in which genetically engineered chaperonin containing a cysteine residue suitable as an adsorption site through thiol mediated linking to nanoparticle was made available to us by NASA-AMES for studies of its adsorption characteristics.

These structurally altered chaperonin rings self-assemble in solution, resulting in a solution containing 2-D arrays. Variable concentrations of this solution containing both individual rings and 2-D self-assembled arrays of chaperonin were adsorbed onto carbon coated TEM grids for different times. TEM imaging showed that 2-D arrays generally showed little affinity toward the carbon surface, although local patches of ordered chaperonin rings can sometimes be observed by carefully searching on the TEM grids (see Fig. A.1). Figure A.2 shows another TEM image of a relatively large patches (~5μm in linear dimension), inside which are regions of locally ordered self-assembled arrays. Two-dimensional Fourier analysis of this image, shown in Fig. A.3, reveals a 2D ordered chaperonin structure. The chaperonin rings within the array had diameters of 17 nm, as expected.

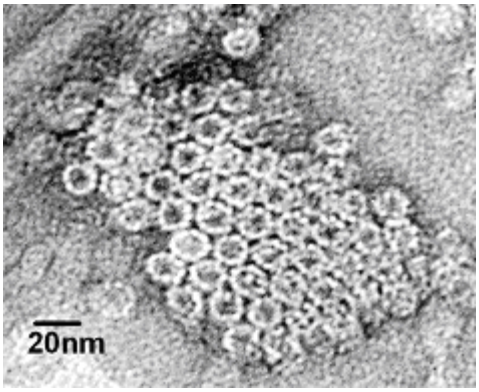

Figure A.1. TEM image of a patch of ordered chaperonin monomers on a carbon coated TEM grid

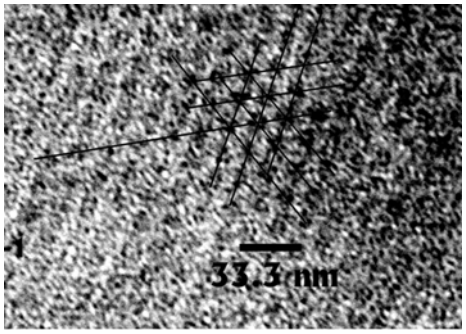

Figure A.2. A TEM image of another area on the sample as in fig. A.1.

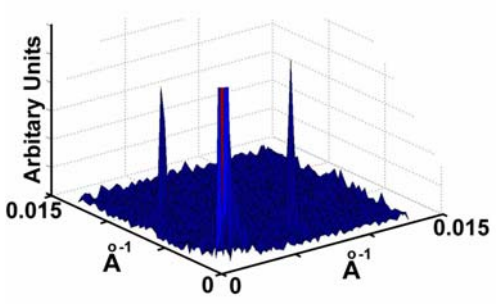

Figure A.3. Two-dimensional Fourier analysis of Figure A.2

- **Protein Adsorption on Solid Surfaces: AFM Studies in Solution**

In continued efforts to achieve enhanced adsorption of chaperonin (oligomeric rings constituted by β subunits of chaperonin TF55 from *Sulfolobus shibatae*) on a solid substrate, self-assembled monolayers are employed to modify the substrate surface. On the outer surfaces of the genetically mutated chaperonin TF55, cysteine amino acids are created. The thiol groups contained in the cysteine residue are utilized as the attachment site to be linked to the halogen end of a SAM modified semiconductor surface (see schematic figure A.4).

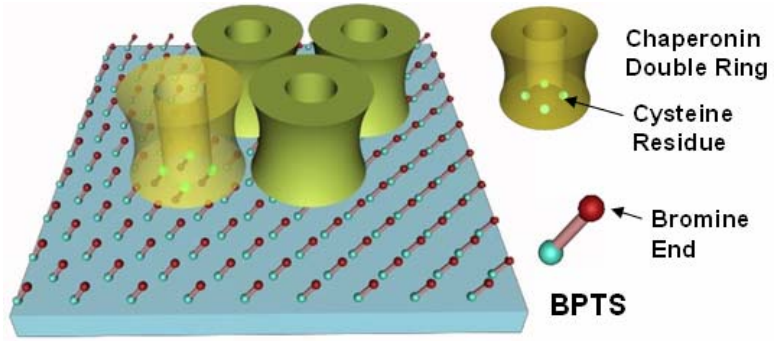

Figure A.4 Schematic showing genetically mutated chaperonins with cysteine amino acid on their outer surfaces being attached to the halogen end (bromine) of the BPTS SAM modified surfaces.

Specifically, for the attachment of mutated chaperonin to silicon substrate, the silicon surface was modified using 3-bromopropyltrichlorosilane (BPTS) SAM with bromine as the free end (for an AFM image of BPTS modified Si surface see section 5, figure 5.1(d)). On BPTS modified silicon surface, 0.075mg/μl of genetically engineered chaperonin in a buffer solution preferred by 2D crystal formation (4mM ATP, 10mM $MgCl_2$, 25mM NaN_3, 25mM HEPES pH7.5) was incubated for 45 minutes at room temperature and then the redundant solution was washed away. AFM image (Fig. A.5) was taken in tapping mode in the same buffer solution. Compared with the reference image of BPTS modified silicon (Fig 5.1d) before incubation of the chaperonin solution, disc-shaped features of diameter ~30nm are observed, as marked in Fig. A.5. These features are consistent with either few-mers formed by aggregation of 3 or 4 chaperonin rings (see figure A.5 inset) or chaperonin rings whose diameter appears to be enlarged because of the AFM tip convolution effect. As seen in the image, the chaperonin almost covers the whole surface. Compared with before utilizing thiol group attachment approach (e.g. the adsorption of

the genetically engineered chaperonin on both hydrophilic mica surface and unmodified silicon surface), the coverage and adsorption rate of genetically engineered chaperonin is significantly increased on the BPTS modified silicon surface.

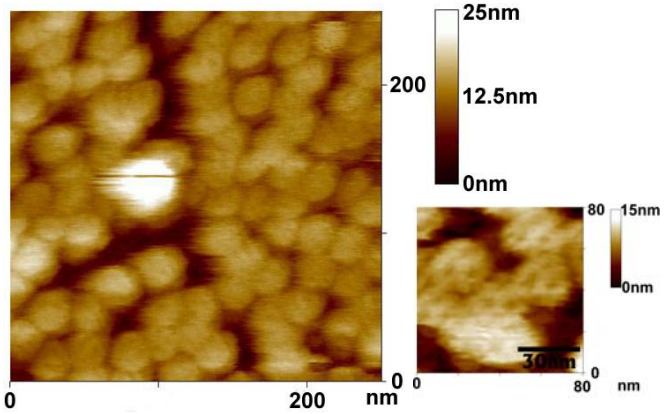

Fig. A.5 AFM image of genetically engineered chaperonin (oligomeric rings constituted by β subunits of chaperonin TF55 from Sulfolobus Shibatae) adsorbed on 3-bromo-propyl-trichlorosilane SAM modified silicon surface. Inset: higher resolution AFM image shows that disc-shaped ~30nm diameter feature could be few-mers formed by aggregation of 3 or 4 chaperonin rings.

II. B. Overgrowth of InAs Self-Assembled Island Quantum Dots on Buried InAs NCQDs as Templates : (Madhukar, Lu, Konkar)

In the preceding, under Major Accomplishment 2, we showed the integration of InAs NCQDs with an as-synthesized diameter of ~4nm. These studies showed that the GaAs overgrowth was of good structural and optical quality. The smaller 4nm InAs NCQDs, however, were prone to evaporation during the high temperature H-radical assisted cleaning that is performed prior to the epitaxical overgrowth. The average NCQDs size after the cleaning is ~ 1nm or lower. At this size scale, it became extremely challenging to get an unambiguous structural or optical signature for their existence using the tools available to us. Hence, we investigated integration of large, as-synthesized, 8nm diameter InAs NCQDs with GaAs via epitaxical overgrowth. To retain the largest NCQD average size after the cleaning, we further optimized the cleaning condition for this new batch of 8nm InAs NCQDs. We find that owing to a much improved quality of the colloidal solution, exclusive thermal cleaning with the same temperature/time combination as used previously but without the H-radical was adequate to realize a sufficiently clean surface.

A key objective of our studies of overgrowth on NCQDs adsorbed on surface was to examine whether the buried InAs NCQDs can act as templates, as opposed to stressors, which can then guide the spatial location of the 3D island self-assembled quantum dots that form upon subsequent InAs deposition. Studies were initiated examining the use of NCQDs as templates. Figure B.1 shows an AFM image of such a sample in which 6nm GaAs is overgrown on thermally cleaned InAs NCQDs and subsequently 2ML InAs is deposited for the formation of InAs SAQDs. The image shows two types of features: the bright spots are the InAs SAQDs and the dark spots are pits. The surface density of the pits is close to the surface density of the as deposited NCQDs. Moreover, the AFM measurements show that the depth of the pits is close to

6nm, the same as the GaAs overgrowth thickness. Independent cross-sectional TEM studies, confirm the presence of ~6nm deep holes (fig.B.2a).

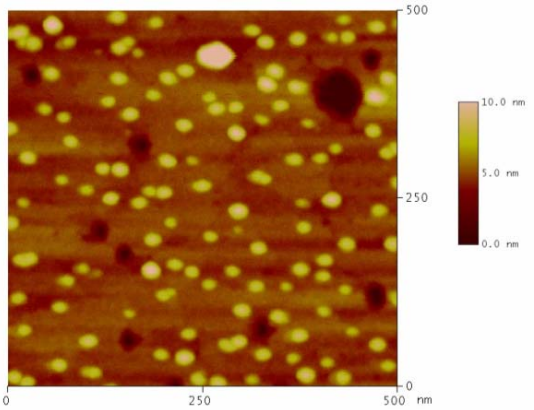

Fig. B.1 AFM image of a sample with 6nm GaAs overgrown on NCQDs.

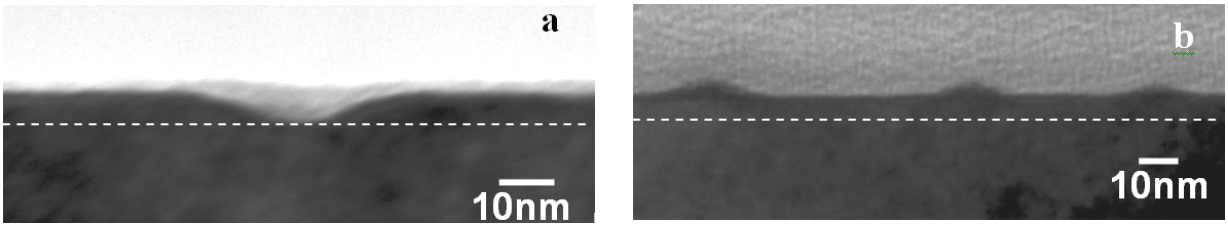

Fig. B.2. XTEM images of the sample taken across a pit (panel a) and from region across InAs SAQDs (panel b). The dotted line in both panels indicates the surface at the beginning of the 6nm GaAs MEE deposition.

AFM examination of sister sample involving the same NCQD deposition and thermal cleaning protocols but with no GaAs overgrowth showed the average NCQD size to be reduced to ~2nm. Thus the above noted AFM and TEM findings on the overgrown GaAs sample would be consistent with the presence of reduced size InAs NCQDs that, owing to the lattice mismatch with GaAs, act to drive the arriving Ga atoms to migrate away during MEE overgrowth (analogous to the Ga migration behavior for MEE overgrowth on the InAs 3D island self-assembled quantum dots, first demonstrated by us [Xie et al. App. Phys. Letts. 65, 2051, (1994)]. In fig.B.1, note that the growth of only 6nm GaAs has led to the formation of a surface that is smooth enough for the subsequent formation of InAs SAQDs. Figure B.2(b) shows a cross-section across InAs SAQDs, the structural quality of the 6nm GaAs MEE overgrowth and the subsequently deposited InAs SAQDs is seen to be defect-free.

III. Personnel Supported

E. Kim (PhD. USC); S. Lu (PhD, USC); S. Vemparala (PhD, LSU); Dave Zaziski (PhD, UCB); D. Aruguete (UCB); M. Ho (MS, USC); Y. Zhang (MS, USC); J. Yao (MS, USC); A. Bansal (MS, USC); T. Asano (USC); Z. Lingley (USC); S. Hughes (UCB); A. Fu (UCB);

Postodcs

Z. H. Chen (USC); M. Makeev (USC); J. Chu (UCB); D. Milliron (UCB); L. Manna (UCB);

Y. Cui (UCB); S. Lu (USC); A. Kanaras (UCB);

IV. Publications (Fifty Three)

1. M. A. Makeev and A. Madhukar, "Simulations of atomic level stresses in systems of buried Ge/Si islands", *Phys. Rev. Lett.* **86**, 5542 (2001).
2. M. Makeev and A. Madhukar, "Large-scale atomistic simulations of atomic displacements, stresses, and strains in nanoscale mesas: Effect of mesa edges, corners, and interfaces," *Appl. Phys. Lett.* **81**, 3789 (2002).
3. A. Nakano, R. K. Kalia, P. Vashishta, T. J. Campbell, S. Ogata, F. Shimojo, and S. Saini, "Scalable atomistic simulation algorithms for materials research," *Scientific Programming* **10**, 263-270 (2002).
4. S. Ogata, F. Shimojo, A. Nakano, P. Vashishta, and R. K. Kalia, "Hybrid quantum mechanical/molecular dynamics simulation on parallel computers: density functional theory on real-space multigrids," *Computer Physics Communications* **149**, 30-38 (2002).
5. J. P. Rino, A. Chatterjee, I. Ebbsjö, R. K. Kalia, A. Nakano, F. Shimojo, and P. Vashishta, "Pressure induced structural transformation in gallium arsenide: a molecular-dynamics study," *Physical Review B* **65**, 195206:1-5 (2002).
6. A. Sharma, P. Miller, X. Liu, A. Nakano, R. K. Kalia, P. Vashishta, W. Zhao, T. J. Campbell, and A. Haas, "Immersive and interactive exploration of billion-atom systems," in *Proceedings of IEEE Virtual Reality 2002 Conference* (IEEE Computer Society, Los Alamitos, CA, 2002) pp. 217-223.
7. X. Liu, A. Sharma, P. Miller, W. Zhao, A. Nakano, R. K. Kalia, and P. Vashishta "Improving interactivity of a parallel and distributed immersive walkthrough application for very large datasets with artificial neural-network-based machine learning," in *Proceedings of the International Conference on Parallel and Distributed Processing Techniques and Applications*, Vol. IV (CSREA Press, Las Vegas, NV, 2002) pp. 2054-2058.
8. P. Vashishta, R. K. Kalia, and A. Nakano, "Info-bio-nano interface: high-performance computing and visualization," in *Proceedings of High Performance Computing* - HiPC 2002, edited by S. Sahni, V. K. Prasanna, and U. Shukla (Springer, Berlin, 2002) pp. 3-8.
9. L. Van Brutzel, C. L. Rountree, R. K. Kalia, A. Nakano, and P. Vashishta, "Dynamic fracture mechanisms in nanostructured and amorphous silica glasses: million-atom molecular dynamics simulations," *Materials Research Society Symposium Proceedings* **703**, V.3.9.1-V.3.9.6 (2002).
10. P. Vashishta, R. K. Kalia, S. Kodiyalam, E. Lidorikis, A. Nakano, P. Walsh, M. E. Bachlechner, T. J. Campbell, S. Ogata, and F. Shimojo, "Multimillion atom simulations of nanosystems on parallel computers," in *Proceedings of the International Symposium on Computational Science and Engineering* 2002, edited by A. Ukawa (Japan Society for the Promotion of Science, Tokyo, Japan, 2002).

11. S. Ogata, F. Shimojo, A. Nakano, P. Vashishta, and R. K. Kalia, "Multiscale materials simulation: a hybrid quanum-classical approach," *Transactions of the Materials Research Society* of Japan 27, 297-300 (2002).

12. L. Manna, E.C. Scher, L. Li, and A. P. Alivisatos, "Epitaxial Growth and Photochemical Annealing of Graded CdS/ZnS Shells on Colloidal CdSe Nanorods", *J. Am. Chem. Soc.*, **124** 7136-7145 (May 2002).

13. L. Manna, E.C. Scher, and A.P. Alivisatos, "Shape Control of Colloidal Semiconductor Nanocrystals," *Cluster Sci.* 13, 521(2002).

14. D. Zanchet, C. M. Micheel, W. J. Parak, D. Gerion, S. C. Williams, A. P. Alivisatos, "Electrophoretic and structural studies of DNA-directed Au nanoparticle groupings." J. Phys. Chem. B, 106, 11758-11763 (2002).

15. H. Kikuchi, R. K. Kalia, A. Nakano, P. Vashishta, H. Iyetomi, S. Ogata, T. Kouno, F. Shimojo, K. Tsuruta, and S. Saini, "Collaborative simulation Grid: multiscale quantum-mechanical/classical atomistic simulations on distributed PC clusters in the US and Japan," in *Proceedings of Supercomputing* 2002 (ACM, New York, NY, 2002).

16. M. A. Makeev, W. Yu, and A. Madhukar, "Stress distributions and energetics in the laterally ordered systems of buried pyramidal Ge/Si(001) islands: An atomistic simulation study," *Phys. Rev. B* **68**, 195301 (2003).

17. M. A. Makeev and A. Madhukar, "Stress and strain fields from an array of spherical inclusions in semi-infinite elastic media: Ge nanoinclusions in Si," *Phys. Rev. B* **67**, 073201 (2003).

18. P.S. Branicio, R. K. Kalia, A. Nakano, J. P. Rino, F. Shimojo, and P. Vashishta, "Structural, mechanical, and vibrational properties of $Ga_{1-x}In_xAs$ alloy: a molecular dynamics study," *Applied Physics Letters* **82**, 1057-1059 (2003)

19. P. S. Branicio, J. P. Rino, F. Shimojo, R. K. Kalia, A. Nakano, and P. Vashishta, "Molecular dynamics study of structural, mechanical, and vibrational properties of crystalline and amorphous Ga1-xInxAs alloy," *Journal of Applied Physics* **94**, 3840-3848 (2003).

20. X. Su, R. K. Kalia, A. Nakano, P. Vashishta, and A. Madhukar, "InAs/GaAs square nanomesas: multimillion-atom molecular dynamics simulations on parallel computers," *J. Appl. Phys.* **94**, 6762 (2003).

21. P. Vashishta, R. K. Kalia, and A. Nakano, "Multimillion atom molecular dynamics simulations of nanoparticles on parallel computers," *Journal of Nanoparticle Research* **5**, 119-135 (2003).

22. A. Nakano, T. J. Campbell, R. K. Kalia, S. Kodiyalam, S. Ogata, F. Shimojo, X. Su, and P. Vashishta, "Scalable multiresolution algorithms for classical and quantum molecular dynamics with applications to nanosystems," in *Handbook of Numerical Analysis*, Volume X, Computational Chemistry, edited by C. Le Bris (Elsevier, Amsterdam, The Netherlands, 2003) pp. 639-666.

23. A. Nakano and J. X. Chen, "High-dimensional data acquisition, computing, and visualization II," *IEEE Computing in Science and Engineering* **5**, 14-15 (2003).

24. A. Sharma, A. Nakano, R. K. Kalia, P. Vashishta, S. Kodiyalam, P. Miller, W. Zhao, X. Liu, T. J. Campbell, and A. Haas. "Immersive and interactive exploration of billion-atom systems," *Presence: Teleoperators and Virtual Environments* **12**, 85-95 (2003).

25. A. Sharma, R. K. Kalia, A. Nakano, and P. Vashishta, "Large multidimensional data visualization for materials science," *IEEE Computing in Science and Engineering* 5, 26-33 (2003).

26. J. X. Chen and A. Nakano, "High-dimensional data acquisition, computing, and visualization," *IEEE Computing in Science and Engineering* **5**, 12-13 (2003)

27. S. Ogata, T. J. Campbell, R. K. Kalia, A. Nakano, P. Vashishta, and S. Vemparala, "Scalable and portable implementation of the fast multipole method on parallel computers," *Computer Physics Communications* **153**, 445-461 (2003).

28. H. Kikuchi, R. K. Kalia, A. Nakano, P. Vashishta, F. Shimojo, and S. Saini, "Scalability of a low-cost multi-Teraflop Linux cluster for high-end classical atomistic and quantum mechanical simulations," in *Proceedings of the 2003 International Parallel and Distributed Processing Symposium* (IEEE/ACM, Nice, France, 2003).

29. E. C. Scher, L. Manna, and A.P. Alivisatos, "Shape Control and Application of Nanocrystals," *Philosophical Transactions of The Royal Society of Chemistry, London A*, **361**, 241-257 (2003).

30. L. Manna, D.J. Milliron, A. Meisel, E.C. Scher, and A.P. Alivisatos, "Controlled Growth of Tetrapod-Branched Inorganic Nanocrystals," *Nature Mat.*, **2**, 382-385 (2003).

31. S. Ogata, T. J. Campbell, R. K. Kalia, A. Nakano, P. Vashishta, and S. Vemparala, "Scalable and portable implementation of the fast multipole method on parallel computers," *Computer Physics Communications* **153**, 445-461 (2003).

32. H. Kikuchi, R. K. Kalia, A. Nakano, P. Vashishta, F. Shimojo, and S. Saini, "Scalability of a low-cost multi-Teraflop Linux cluster for high-end classical atomistic and quantum mechanical simulations," in *Proceedings of the 2003 International Parallel and Distributed Processing Symposium* (IEEE/ACM, Nice, France, 2003).

33. Y. Cui, M. T. Bjork, J. A. Liddle, C. Sonnichsen, B. Boussert, and A. P. Alivisatos, "Integration of Colloidal Nanocrystals into Lithographically Patterned Devices", *Nano Letters*, **4**, 1093 (2004).

34. Aihua Fu, C. M. Micheel, J. Cha, H. Chang, H. Yang, and A. P. Alivisatos, "Discrete Nanostructures of Quantum Dots/Au with DNA", *Journal of American Chemical Society*, **126**, 10832 (2004).

35. M. A. Makeev, W. Yu, and A. Madhukar, "Atomic scale stresses and strains in Ge/Si(001) nanopixels: an atomistic simulation study," *J. Appl. Phys.* **96**, 4429 (2004).

36. S. Vemparala, B. B. Karki, R. K. Kalia, A. Nakano, and P. Vashishta, "Large-scale molecular dynamics simulations of alkanethiol self-assembled monolayers," *J. Chem. Phys.* **121**, 4323 (2004).

37. S. Vemparala, R. K. Kalia, A. Nakano, and P. Vashishta, "Electric field induced switching of poly (ethylene glycol) (PEG) terminated self-assembled monolayers: a parallel molecular dynamics simulation," *J. Chem. Phys.* **121**, 5427 (2004).

38. S. Kodiyalam, R. K. Kalia, A. Nakano, and P. Vashishta, "Multiple grains in nanocrystals: effect of initial shape and size on transformed structures under pressure," *Phys. Rev. Lett.* **93**, 203401 (2004).

39. F. Shimojo, S. Kodiyalam, I. Ebbsjö, R. K. Kalia, A. Nakano, and P. Vashishta, "Atomistic mechanisms for wurtzite-to-rocksalt structural transformation in cadmium selenide under pressure," *Phys. Rev. B* **70**, 184111 (2004).

40. A. Konkar, S. Lu, A. Madhukar, S. M. Hughes, and A. P. Alivisatos, "Semiconductor nanocrystal quantum dots on single crystal semiconductor substrates: high resolution transmission electron microscopy," *Nano Lett.* **5**, 969 (2005).

41. A. Madhukar, S. Lu, A. Konkar, Y. Zhang, M. Ho, S. Hughes, and A. P. Alivisatos, "Integrated semiconductor nanocrystal and epitaxical nanostructure systems: structural and optical behavior," *Nano Lett.* **5**, 479 (2005).

42. T. J. Campbell, G. Aral, S. Ogata, R. K. Kalia, A. Nakano, and P. Vashishta , "Oxidation of aluminum nanoclusters," *Phys. Rev. B* **71**, 205413 (2005).

43. S. Khatsevich, D. H. Rich, E. T. Kim, and A. Madhukar, "Cathodoluminescence imaging and spectroscopy of excited states in InAs self-assembled quantum dots," *J. Appl. Phys.* **97**, 123520 (2005).

44. F. Shimojo, R. K. Kalia, A. Nakano, and P. Vashishta, "Embedded divide-and-conquer algorithm on hierarchical real-space grids: parallel molecular dynamics simulation based on linear-scaling density functional theory," *Comp. Phys. Comm.* **167**, 151 (2005)

45. M. A. Makeev, R. K. Kalia, A. Nakano, P. Vashishta, and A. Madhukar, "Effect of geometry on the stress relaxation in InAs/GaAs rectangular nano-mesas: Multimillion-atom molecular dynamics simulations," *J. Appl. Phys.* **98**, 114314 (2005).

46. C. Sonnichsen, B. Reinhard, J. Liphardt, and A. P. Alivisatos, 'A molecular ruler based on plasmon coupling of single gold and silver nanopartivles", *Nature Biotechnology* , **23**, 741 (2005)

47. Y. Cui, U. Banin, M. T. Bjork, and A. P. Alivisatos, "Electrical transport through a single nanoscale semiconductor branch point," *Nano Letters* **5**, 1519 (2005).

48. N. J. Lee, R. K. Kalia, A. Nakano, and P. Vashishta, "Pressure-induced structural transformations in cadmium selenide nanorods" *Applied Physics Letters* **89**, 093101: 1 (2006).

49. M. Makeev, A. Madhukar, "Calculation of vertical correlation probability in Ge/Si(001) shallow island quantum dot multilayer systems", *Nano Letters* **6**, 1279 (2006).

50. S. Lu, A. Bansal, W. Sassou, T. Berger, and A. Madhukar, Receptor-Ligand –Based Specific cell Adhesion on Solid Surfaces: Hippocampal Neuronal Cells on Bilinker Functionalized Glass", *Nano Letters* **6**, 1977 (2006).

51. A. Fu, W. Gu, B. Boussert, K. Koski, D. Gerion, L. Manna, M. LeGros, C. A. Larabell, and A. P. Alivisatos, "Semiconductor Quantum Rods as Single Molecule Florescent Biological Labels" *Nano Letters* **7**, 179 (2007).

52. D. M. Aruguete, M. A. Marcus, L.-S. Li, A. Williamson, S. Fakra, F. Gygi, G. Galli, and A. P. Alivisatos, "Surface Structure of CdSe Nanorods Revealed by Combined X-ray Absorption Fine Structure Measurements and ab Inito Calculations," *J. Phys. Chem. C*, **111**, 75 (2007).

53. S. Lu, A. Madhukar, "Nonradiative resonant excitation transfer from nanocrystal quantum dots to adjacent quantum channels", *Nano Letters*, **7**, 3443 (2007).

V. Interactions/Transitions (Conferences; Industry; etc.)

1. A. Madhukar, "Semiconductor Nanostructure: Nature's Way", International Conf. on Nanotechnology, Taiwan (Nov. 2001)
2. A. Madhukar, "Stress-Engineering and Biochemical Template Driven Semiconductor Quantum Dot Array", Indian Inst. of Tech. Bombay (Dec. 27, 2001, Kaupur (Jan. 3, 2002); Indian Inst. of Science, Molecular Biology Division (Jan. 7, 2002)
3. D.H. Rich, C. Zhang, I. Mukhametzhanov, and A. Madhukar, "Cathodoluminescence study of cluster size variations in InAs/GaAs self-assembledquantum dots", Annual meeting of the Israel Physical Society, (December 2001).
4. A. P. Alivisatos, "Polymer Colloids", Manchester, Gordon Research Conference, New Hampshire (July 2001).
5. A. P. Alivisatos, "Clusters, Nanocrystals & Nanostructures", Gordon Research Conference, New London, Connecticut (July 2001)
6. A. P. Alivisatos, (Graduate student, Erik Scher, attended and presented conference paper on behalf of principal investigator.), Royal Society of Chemistry, Birmingham, England (July 2001).
7. A. P. Alivisatos, "Inorganic Nanorods: Synthesis, Alignment, Properties," American Chemical Society National Meeting, Chicago, IL. (August 2001).
8. A. P. Alivisatos, "Polymer/Nanocrystal Photovoltaics," with Prof. J. Frechet. UPS-2001, Les Diablerets, Switzerland (September 2001).
9. A. P. Alivisatos, "Quantum Rods: Building Blocks for New Liquid Crystals and Photovoltaics," Corning's Nanotechnology Innovation Workshop, Elmira, New York; and Kilpatrick Lecturer, Illinois Institute of Technology, Chicago, Illinois (October. 2001).
10. A. P. Alivisatos, "Inorganic Nanorods: Synthesis, Alignment, Properties," International Vacuum Congress, San Francisco, California (October. 2001).
11. A. P. Alivisatos, "Inorganic Nanorods: Synthesis, Properties, Applications," Princeton University, Newark, New Jersey and University of Pennsylvania, Philadelphia, Pennsylvania (November, 2001).
12. A. P. Alivisatos, "Inorganic Nanorods: Synthesis, Properties, Applications," Weissberger/Williams Lecturer, Eastman Kodak Company, Rochester, New York (November, 2001).

13. A. P. Alivisatos, “Inorganic Nanorods: Synthesis, Properties, Applications,” Nanotech Plane Conference, and Material Research Society Fall Meeting, Boston, Massachusetts (November, 2001).
14. A. P. Alivisatos, – Plenary Lecturer, "X-Ray Diffraction and Spectroscopy as Tools for the Study of Inorganic Nanocrystals,” Roentgen Symposium, University of Wuerzurg, Wuerzburg, Germany (December, 2001).
15. A. P. Alivisatos, Noyes Distinguished Lecturer, “Inorganic Nanorods: Synthesis, Properties, Applications,” University of Texas at Austin, Texas (January, 2002).
16. A. P. Alivisatos, “Inorganic Nanorods: Synthesis, Properties, Applications,” Harvard/MIT Physical Chemistry Seminar, Boston, Massachusetts (February, 2002).
17. A. P. Alivisatos, Invited Speaker, University of Washington General Colloquium, Seattle Washington (March, 2002).
18. A. P. Alivisatos, “Soft X-Ray Absorption Spectroscopy of Single Nanocrystals,” American Physical Society Meeting, Indianapolis, Indiana (March, 2002).
19. A. P. Alivisatos, “Inorganic Nanorods: Synthesis, Alignment, Properties,” Spring 2002 MRS Meeting, San Francisco, California (April, 2002).
20. A. P. Alivisatos, Invited Speaker, UCSB Technology Forum on Self-Assembly in Nanomaterials and Devices, University of California, Santa Barbara, California (April, 2002)..
21. A. P. Alivisatos, Invited Speaker, Award Ceremony for the 2001 Baekland Medal, Rutgers University, New Brunswick, New Jersey (April, 2002).
22. A. P. Alivisatos, Marcus Lecturer, Department of Chemistry, Washington University, St. Louis, Missouri (May, 2002).
23. A. P. Alivisatos, “Inorganic Nanorods: Synthesis, Properties, Photovoltaic Applications,” Atofina Chemicals, Philadelphia, Pennsylvania (May, 2002).
24. A. P. Alivisatos,– Nanotechnology Conference, UCLA Nanosystems Institute, Los Angeles, California (July, 2002).
25. A. P. Alivisatos, CNSI, University of California at Santa Barbara, Santa Barbara, California (July, 2002).
26. A. P. Alivisatos, Plenary Lecture: “Inorganic Nanorods: Synthesis, Properties, Photovoltaic Applications,” 14th International Conference on Photochemical Conversion and Storage of Solar Energy, Sapporo, Japan (August, 2002).
27. A. P. Alivisatos, “Inorganic Nanorod Liquid Crystals,” ACS Meeting, Ordered Molecular Assemblies of Nanoparticles Symposium, Boston, Massachusetts (August 2002).
28. A. P. Alivisatos, “Inorganic Nanorods: Synthesis, Properties, Photovoltaic Applications,” S P R C Meeting, Stanford University, Palo Alto, California (September 2002).
29. A. P. Alivisatos, “Nanocrystals as a New Class of Macromolecule,” C S E M Annual Meeting, California Technical Institute, Pasadena, California (September 2002).

30. A. P. Alivisatos, “Colloidal Quantum Dots,” Second Annual Conference on Semiconductor Quantum Dots, The University of Tokyo, Komaba, Tokyo, Japan (September, 2002).
31. A. P. Alivisatos, “Inorganic Nanorods: Synthesis, Properties, Applications,” CNSI, UCLA Nanosystems Seminar Series, :Los Angeles, California (October 2002).
32. A. P. Alivisatos, “Nanocrystals as a New Class of Macromolecule,” Korea Conference on Innovative Science and Technology: Nanotechnology Future Implications, Jeju Island, Korea (November, 2002).
33. A. P. Alivisatos, “Inorganic Nanorods: Synthesis, Properties, Applications,” MRS Fall 2002 Meeting, Boston, Massachusetts (December, 2002).
34. A. P. Alivisatos, “Inorganic Nanorods: Synthesis, Properties, Applications,” Condensed Matter Meeting of the Dutch Foundation for Fundamental Research on Matter, Veldhoven, The Netherlands (December, 2002).
35. A. P. Alivisatos, “Nanocrystals as a New Class of Macromolecule,” The Iowa State Hansen Lectures, Des Moines, Iowa (January, 2003).
36. A. P. Alivisatos, “Application of Colloidal Quantum Dots to Cell Tracking and Assessment of Metastatic Potential in Cancers,” American Association for the Advancement of Science, Big Things in Little Packages Nanotechnology Seminar, Denver, Colorado (February, 2003 – 2003).
37. A. P. Alivisatos, “Biomedical Applications of Nanocrystals”, Plenary speaker at the American Association for Dental Research, San Antonio,Texas (March 2003).
38. A. P. Alivisatos, “Selective Adhesion Method for Nanocrystal Shape Control”, American Chemical Society Spring 2003 Meeting, New Orleans, LA (March 23-27, 2003).
39. P. Vashishta, “Multimillion Atom Simulations of Nanosystems and Interfaces on Parallel Computers,” "International Conference on Non-Crystalline Inorganic Materials-Synthesis, Structure and Simulation (CONCIM)”, Bonn, Germany, (April, 2003).
40. P. Vashishta, “Multimillion Atom Simulations of Nanosystems on Parallel Computers - Nanophase Materials, Nanopixel, Nanoindentation and Oxidation,” "Modeling and Simulation in Micro and Nano Technologies and Materials Engineering" Toulouse, France, (April, 2003).
41. A. Nakano, “Grid-enabling multiscale simulations,” Mardi Gras 2003 Conference on “Experiments and Simulations at Nano-Bio Interface and Frontiers of Grid Computing”, Baton Rouge, LA (February, 2003).
42. P. Vashishta, “Info-Bio-Nano Interface: High-Performance Computing & Visualization,” “Computational Science Workshop for Underrepresented Groups", LSU@Baton Rouge, LA, (January, 2003).
43. P. Vashishta, “Info-Bio-Nano Interface: High-Performance Computing & Visualization,” “High Performance Computing 2002", Bangalore, India, (December, 2002).
44. A. Nakano, “Collaborative simulation Grid: multiscale quantum-mechanical/classical atomistic simulations on distributed PC clusters in the US and Japan,” IEEE/ACM Supercomputing 2002, Baltimore, MD (November, 2002).

45. P. Vashishta, “Multimillion Atom Simulations of Nanosystems on Parallel Computers - Nanopixel, Nanoindentation and Oxidation of Aluminum Nanoparticles,” “CNER-MSI Nanosimulation Workshop” Center for NanoEnergetics Research Minnesota Supercomputing Institute, Minneapolis, MN, (August, 2002).
46. P. Vashishta, “Multimillion Atom Simulations of Nanosystems on Parallel Computers - Nanopixel, Nanoindentation and Oxidation,” "APS Conference on Computational Physics 2002", San Diego, CA, (August, 2002).
47. R. Kalia, “Massively Parallel, Multiscale Simulations of Nanostructured Materials,” CIMTEC 2002, Florence, Italy (July, 2002).
48. P. Vashishta, “Amorphous Materials in Various Incarnations,” “CECAM Workshop on Atomic Structure and Transport in Glassy Networks”, Lyon, France, (June, 2002).
49. P. Vashishta, “Billion-atom Multiscale Simulations on a Grid,” "NSF DMR Computational Materials Theory Program Review", Urbana, IL, (June, 2002).
50. P. Vashishta, “Large-Scale Molecular Dynamics Simulations of the Oxidation of Metallic Nanoparticles,” "Gordon Conference on Energetic Materials", Tilton, NH, (June, 2002).
51. A. Nakano, R. K. Kalia, and P. Vashishta, “Multiscale fracture and nanoindentation simulations and visualization,” DoD High Performance Computing Users Group Conference, Austin, TX (June, 2002).
52. R. Kalia, “Multiscale Fracture and Nanoindentation Simulations and Visualization,” DoD High-Performance Computing Users Group Conference, Austin, TX (June, 2002).
53. R. Kalia, “Multiscale Simulation of Atomistic Processes in Nanostructured Materials,” NSF Workshop, University of Illinois at Urbana-Champaign, (June, 2002).
54. A. Madhukar, “Semiconductor Nanostructures: Nature’s Way,” Indian Institute of Technology, Bombay, India (December, 2002).
55. A. Madhukar, “Directed Assembly of Semiconductor Nanostructures,” Raman Research Institute, Banglore, India (December, 2002).
56. A. Madhukar, “Stress-Engineered Quantum Dots,” Indian Institute of Technology, Madras, India (January, 2003).
57. A. Madhukar, “Nanocrystal and Epitaxical Semiconductor Quantum Dots,” Jawaharlal Nehru Institute, Banglore, India (January, 2003).
58. A. Madhukar, “Quantum Dot Arrays: Nature’s Way,” Mardi Gras Conference, Baton Rouge, LA (February 2003).
59. A. Madhukar, “Self-Assembled Epitaxical Nanostructure Arrays,” American Physical Society March Meeting, Austin, Texas (March 2003).
60. A. P. Alivisatos, “Clusters, Nanocrystals and Nanostructures”, Gordon Conference, Connecticut College, New London, CT, (August 2003).
61. A. P. Alivisatos, IEEE Nano 2003, San Francisco, California, (August 2003).

62. A. P. Alivisatos, “Liquid Crystalline phases of Anisotropic Inorganic Crystals”, ACS 2003, Physical Science Division, Physical Chemistry of Complex Fluids Symposium, New York City, New York, (September 2003).
63. A. P. Alivisatos, “Optical, Electrical, and Thermodynamical Properties of a New Class of Materials, Semiconductor Nanocrystals”, IUMRS-CAM 2003, Yokohama, Japan, (October 2003).
64. A. P. Alivisatos, :Nontraditional Approaches to Patterning” Fall Meeting of the MRS, Boston, Masschusetts, (December 2003).
65. A. P. Alivisatos, “Quantum Dots and their application in Biomedicine”, Pittcon Conference, Biomedical Applications of Nanotechnology and Nanodevices Symposium, Chicago, Illinois (March 2004).
66. A. P. Alivisatos, “Magnetic and Semiconducting Nanorods”, American Physical Society March Meeting, Montreal, Canada (March 2004).
67. A. P. Alivisatos, “Electrical Studies of Branched Semiconductor Nanocrystals with Applications in Chemical Sensing”, “Integration of colloidal nanocrystals into electrical devices”, “Nanoscience in Inorganic Chemistry Nanotech and the Environment Biochemical Aspects of Nanoscience” Spring ACS Meeting, Anaheim, California (March 2004).
68. A. P. Alivisatos, “Advanced Microsystems-Integration with Nanotechnology and Biomaterials Symposium on 3D Nanoengineered Assemblies”, MRS Spring Meeting, San Francisco, California (April 2004):
69. A. P. Alivisatos, National Cancer Institute Spore Investigator’s Workshop, Washington D.C. (July 11, 2004).
70. A. P. Alivisatos, The Gordon Research Conference on Nanostructure Fabrication, Tilton, NH (July 17-19, 2004).
71. A. P. Alivisatos, The Gordon Research Conference on Electronic Processes in Organic Materials, Mount Holyoke College, South Hadley, MA (July, 2004).
72. A. P. Alivisatos, High Pressure Semiconductor Physics Conference, Berkeley, CA (August, 2004).
73. A. P. Alivisatos, The Gordon Research Conference on Chemistry at Interfaces, Kimball Union Academy, New Hampshire (August, 2004).
74. A. P. Alivisatos, “Biophysical chemistry and novel imaging of single molecules and single cells,” ACS National Meeting, Philadelphia, PA (August, 2004).
75. A. P. Alivisatos, “Colloidal QDs and applications to biological tags,” the 2004 Monte Verita Summer School on Semiconductor Quantum Dots: From Physics to Devices, Ascona, Switzerland (September, 2004).
76. A. P. Alivisatos, Lectureship Award at the 57th Divisional Meeting of Colloid and Interface Chemistry, The Chemical Society of Japan, Yamaguchi, Japan (September, 2004).
77. A. P. Alivisatos, Professorship, the Linnett Lectures, Cambridge, England (October 11-18, 2004).

78. A. P. Alivisatos, The Chemistry/Biochemistry Department Seminar, San Francisco State University, San Francisco, CA (November, 2004).

79. A. P. Alivisatos, Lecturer, 2004-2005 Kolthoff Lecturer, Department of Chemistry, University of Minnesota, Twin Cities, Minneapolis, MN (November, 2004).

80. A. P. Alivisatos, "Micron and Nanoscale Materials Interfaced with Biology and Medicine" Fall 2004 MRS Meeting, Philadelphia, PA (November, 2004)..

81. A. P. Alivisatos, Keynote Speaker, Engineering Novel Materials: Computation, Experiment and Theory, Forum sponsored by the University of California Office of the President, Arnold and Mabel Beckman Center of the National Academies, Irvine, CA (March, 2005).

82. A. P. Alivisatos, "New nanocrystal assemblies for photonic structures," "Structural and chemical transformations in colloidal nanocrystals," "Charging and electrical transport through individual nanocrystal tetrapods," The ACS Spring Meeting, San Diego, CA (March, 2005)

83. A. P. Alivisatos, Michigan State Seminars, Lansing, MI (April, 2005).

84. A. P. Alivisatos, "Chemical transformations of nanocrystals," MRS Spring Meeting, San Francisco, CA (Spring, 2005).

85. A. P. Alivisatos, "Colloidal nanocrystals: synthesis, properties and applications," Symposium: The Berkeley in Silicon Valley, The Sun Microsystems Santa Clara Conference Center, Santa Clara, CA (May, 2005).

86. A. P. Alivisatos, "New nanocrystal assemblies for use in cancer research," Plenary Speaker, National Cancer Institute Symposium Nanotech 2005 Invitation, 2005 Nanotechnology Conference and Trade Show, Anaheim, CA (May, 2005).

87. A. P. Alivisatos, Seminar series within Special Program in Bioscience, Chalmers University of Technology and Goteborg University (May, 2005).

88. R. Kalia, "Large-scale atomistic simulations of nanoindentation and crack propagation under compression," DoD-HPCMP 2004 User Group Conference, Williamsburg, VA (June, 2004).

89. P. Vashishta, "Billion-atom multiscale simulations of nanosystems on a grid," NSF Division of Materials Research ITR Computational Workshop, University of Illinois, Urbana, IL (June, 2004).

90. R. Kalia, "De Novo computational design of optimum materials," Service de Physique et de Chimie des Surfaces et Interfaces, CEA-Saclay, France (July, 2004).

91. P. Vashishta, "Ultrascale simulations high performance computing and visualization," DARPA Workshop on Metaphoric Optical Computing, San Diego, CA (July, 2004).

92. A. Nakano, "High-end multiscale simulations of nanomaterials," ECCOMAS European Congress on Computational Methods in Applied Sciences and Engineering 2004, Jyvaskyla, Finland (July, 2004).

93. P. Vashishta, "Large-scale atomistic simulations of nanosystems on parallel computers," International Conference on Computational Engineering & Science (ICES04), Madeira, Portugal (July, 2004).

94. A. Madhukar, “Strained semiconductor epitaxy: a matter of length and time scales”, 2004 Conference on Computational and Experimental Challenges in Hybrid Physical, Chemical and Biological Systems, Los Angeles, CA (August, 2004)..

95. R. Kalia, “Multiscale simulations of nanostructured ceramics and glasses,” CMT28, Washington University, St. Louis, MO (September, 2004).

96. A. Madhukar, “Heterojunction nano/bio-technology,” UC-Irvine, Irvine, CA (October 2004).

97. R. Kalia, “Hierarchical atomistic simulations of fracture in nanostructured materials,” Lorentz Workshop on the Statistical Physics of Pattern Formation and Fracture in Disordered Materials, Leiden, The Netherlands (November, 2004).

98. R. Kalia, “Large-scale atomistic simulations of dynamic fracture in glasses and ceramics,” 2004 MRS Fall Meeting, Boston, MA (November, 2004).

99. P. Vashishta, “Multimillion atom simulations and visualization of oxidation and hypervelocity impact damage,” 24th Army Science Conference, Orlando, FL (November, 2004).

100. A. Nakano, “Large space-time multiscale simulations of nanosystems,” PRETISSIMO Workshop on Molecular Simulation: Algorithmic and Mathematical Aspects, Paris, France (December, 2004).

101. A. Madhukar, “Nanoscience and nanotechnology”, Computational Science Workshop for Underrepresented Groups (CSWUG), Los Angeles, CA (January 2005).

102. A. Madhukar, “Integrated epitaxical self-assembled and nanocrystal quantum dots: a new paradigm,” SPIE Symposia, San Jose, CA (January, 2005).

103. A. Madhukar, “Strained semiconductor epitaxy: a matter of length and time scales,” TMS Symposium, San Francisco, CA (February, 2005)

104. P. Vashishta, “Multimillion atom simulations of dynamics of oxidation aluminum nanoparticle and hypervelocity impact damage in aluminum nitride ceramic,” American Chemical Society, San Diego, CA (March, 2005).

105. P. Vashishta, “Multimillion atom simulations of nanosystems - structural transformations in nanocrystals and hypervelocity impact damage,” Computational Science Workshop 2005 (CSW2005), Tsukuba, Japan (March, 2005).

106. A. Nakano, “Multimillion-atom molecular dynamics simulation of chemical reactions,” International Conference on Scientific Computing and Differential Equations, Nagoya, Japan (May, 2005).

107. A. Madhukar, “Beyond Epitaxical Self-Assembled and Nanocrystal Quantum Dots: Composite Systems” MRS Fall Meeting, San Francisco (November 2006).

108. A. P. Alivisatos, “The Future of Solar Power Generation,” World Trade Club, San Francisco, California (July 2006).

109. A. P. Alivisatos, “Field Enhancements in Nanoparticle Assemblies, Active Plasmonic Structures and Devices Symposium, Gordon Conference, Keene, New Hampshire (July, 2006).

110. A. P. Alivisatos, Very High Efficiency Solar Cell Program Review Meeting, Herndon, Virginia (August 2006).

111. A. P. Alivisatos, Technical Council Center for Cancer Nanotechnology Excellence, Northwestern University (August, 2006).

112. A. P. Alivisatos, "Chemical Transformation in Nanocrystal," Single Molecule Biophysical Chemistry Symposium, 232nd ACS National Meeting, San Francisco, California (September, 2006).

113. A. P. Alivisatos, Plenary Lecture, "Colloidal Nanocrystals with Applications in Biological Imaging and Renewable Energy," MESA and Institute for Nanotechnology, En Schede, The Netherlands (September, 2006).

114. A. P. Alivisatos, "Chemical Transformations in Nanocrystals," Stanford Chemical Engineering Colloquium, Stanford, California

115. A. P. Alivisatos, "Colloidal Nanocrystals of Complex Shape: Synthesis, Properties, Applications," "Chemical Transformations in Nanocrystals," and "Artificial Molecules Built from Colloidal Nanocrystals," Texas A&M Frontiers Lectures, College Station, Texas (October, 2006).

116. A. P. Alivisatos, "Promises to Keep," Cancer Imaging Symposium, Emerging Technologies, University of California, San Francisco, California (October, 2006).

117. A. P. Alivisatos, "Hybrid-Nanorod Polymer Solar Cells," University of Delaware, Newark, Delaware (October, 2006).

118. A. P. Alivisatos, "Hybrid-Nanorod Polymer Solar Cells," St. Paul, Minnesota (October, 2006).

119. A. P. Alivisatos, "Plasmon Rulers for Measuring Dynamical Distance Changes in Biological Macromolecular Assemblies," SACP, Chemical Transformation in Nanocrystals, Pittsburg, Pennsylvania (November, 2006).

120. A. P. Alivisatos, "Colloidal Nanocrystals of Complex Shape: Synthesis, Properties, Applications," Nanotech Manufacturing, Moscone Center, San Francisco, California (November, 2006).

121. A. P. Alivisatos, "Colloidal Nanocrystals of Complex Shape: Synthesis, Properties, Applications," MRS, Boston, Massachusetts (November, 2006).

122. A. P. Alivisatos, Plenary Lecture, "Nanocrystals and Nanocrystal Molecules as Single Molecule Optical Probes in Biomedical Imaging," and "Nanocrystal Based Solar Cells," at the University of Copenhagen and the Technical University of Denmark (December, 2006).

123. A. P. Alivisatos, "Chemical Transformations in Nanocrystals," Croucher Workshop, ASI, Hong Kong, China (January, 2007).

124. A. P. Alivisatos, "Nanocrystal Solar Cells," Gordon Research Conference on Renewable Energy with Emphasis on Solar Supply, Ventura, California (January, 2007).

125. A. P. Alivisatos, Distinguished Eyring Lecturer, "Nanocrystal Molecules," Arizona State University, Tempe, Arizona (February, 2007).

126. A. P. Alivisatos, “Hybrid-Nanorod Polymer Solar Cells,” 2007 Keystone Symposium on Nanotechnology in Biomedicine, Tahoe City, California (February, 2007).

127. A. P. Alivisatos, “Hybrid-Nanorod Polymer Solar Cells,” and “Structural and Chemical Transformations in Nanocrystals,” in the two symposia: (1) Basic Research in Chemistry and Biochemistry -- Solar Photon Conversion and (2) Dynamics on the Nanoscale -- Quantum Dots; at the ACS National Meeting, Chicago, Illinois (March, 2007).

128. A. P. Alivisatos, “Hybrid-Nanorod Polymer Solar Cells,” MRS Spring Meeting. San Francisco, California (April, 2007).

129. A. P. Alivisatos, Lipscombe Lecturer, “Artificial Molecules Built from Colloidal Nanocrystals,” University of South Carolina, Columbia, South Carolina (April, 2007).

130. A. P. Alivisatos, “Nanoparticle-Based Energy Conversion and Storage,” Gordon Research Conference, Chemistry of Supramolecules and Assemblies, Tuscany, Italy (May, 2007).

131. A. P. Alivisatos, Keynote Speaker, “Nanomaterials and Solar Energy Utilization,” 2007 Cleantech Conference and Trade Show, Santa Clara, California (May, 2007)..

132. S. Lu “Optical Probing of Cell Physiological Changes under Stress”, BMES Annual Meeting, Los Angeles (September 2007).

133. A. Madhukar, “Disease and Translational Nanoscience Platform Paradigms: A Matter of Inversely Related Times”, Translational Nanoscience Conference, Los Angeles (March, 2008).

VI. New Discoveries

1. Controlled synthesis of branched inorganic dendrimers (Alivisatos et.al)

2. Potentially highly efficient nonradiative resonant energy transfer from nanocrystal quantum dots to adjacent high charge carrier mobility transport channels (Lu and Madhukar)

Patent Application Filed

1. S. Lu, A. Madhukar, M. Humayun, “Functional Abiotic Nanosystems”, US Non-provisional Patent Application, Application # 12138289 (2008).
2. A. Madhukar, S. Lu, “Radiative energy conversion to electricity using nonradiative resonant excitation transfer in and from nanoparticle absorbers to adjacent high mobility charge transport channels”, US Provisional Patent Application (2007).